INTEGRATED CHEMOSTRATIGRAPHY AND PALEOCEANOGRAPHY OF THE MISSISSIPPIAN BARNETT FORMATION

by

KRYSTIN CHANTEL ROBINSON

Presented to the Faculty of the Graduate School of

The University of Texas at Arlington in Partial Fulfillment

of the Requirements

for the Degree of

MASTTER OF SCIENCE IN GEOLOGY

THE UNIVERSITY OF TEXAS AT ARLINGTON

December 2012

ACKNOWLEDGEMENTS

First and foremost I would like to thank my advisor, Dr. Harry Rowe, for his time and never ending guidance over the past three years. Without his help, I would not have had the multitude of opportunities given to me, nor would this thesis have ever been possible. I also want to thank the members of my graduate committee, Dr. John Wickham and Dr. Majie Fan. Your patience and guidance both as committee members and professors have greatly molded the geologist I am today.

Second I would like to thank Pioneer Natural Resources for allowing me access to the Pioneer #1 core. Specifically, I would like to thank Mr. Shane Seals, Mr. Andy Stephens, and Mr. Donny Lowery for their unceasing patience and continual support throughout my research. I would also like to specially thank Mr. Stephens for granting me an internship opportunity with Pioneer Natural Resources. The lessons learned during my time at Pioneer, as well as all the advice given have served me well in many of my other endeavors.

I would also like to thank several members of the geochemistry research group. Robert Nikirk, Karen McCreight, and Jessica Buckles provided much assistance in data analysis as well as sanity support when I was standing on the ledge.

I want to thank Mr. Joeseph Wert for his infinite wisdom, support, and endless belief in myself. Without you, my college career would never have been possible. You truly were the best man I have ever known and you will never be forgotten, RIP.

I would also like to thank my friends and family for all of their continued support. Your love and encouragement have given me the support I needed to persevere when I didn't think it possible.

Lastly, I would like to thank my wonderful and amazing husband, Darren Robinson. You have put up with a lot these past years and that has not gone ignored. You are my rock.

December 5, 2012

ABSTRACT

INTEGRATED CHEMOSTRATIGRAPHY AND PALEOCEANOGRAPHY OF THE MISSISSIPPIAN BARNETT FORMATION

Krystin Robinson, M.S.

The University of Texas at Arlington, 2012

Supervising Professor: Harold Rowe

The Barnett Formation was deposited on a gently sloping marine margin that ultimately became the Fort Worth Basin (FWB), a foreland basin that evolved during the late Paleozoic Era. The FWB formed as a result of the early Ouachita Orogeny, due to the collision of Laurasia and Gondwana. The Mississippian (Visean and Serpukhovian) Barnett Formation is an organic-rich lithologic unit composed primarily of laminated siliceous mudrock with some calcareous mudrock intervals. The objective of the project is to develop and interpret stratigraphic changes in the geochemistry of the Barnett Formation for the purposes of understanding the paleoceanography of the northernmost Fort Worth Basin, and refining the stratigraphy for the oil and gas industry. Methods used to carry out the project include: real-time geochemical analysis using x-ray fluorescence (XRF) of the core face, TOC (total organic carbon) and TIC (total inorganic carbon) analysis, and stable carbon isotope analysis of organic and inorganic constituents. The elevated occurrence of redox-sensitive trace elements, including molybdenum, vanadium, zinc and uranium, suggests that periods of anoxia and euxinia (free sulfide) existed during deposition. These conditions likely contributed to a high level of organic preservation. Major elemental components (%Si, %Al, and %Ca) indicate the dominance of

quartz, clay, and calcite, respectively, with the latter dominating the underlying strata (Late Ordovician Viola Formation) and the overlying strata (Forestburg Member). Thin carbonate-rich layers within the Barnett may reflect calcite-rich density flows derived from a nearby carbonate platform (Chappel Limestone). These results add to the general knowledge of the stratigraphy of the Barnett Formation, and provide further support for interpreting well log data and deriving more comprehensive models of depositional environments.

TABLE OF CONTENTS

LIST OF ILLUSTRATIONS

Figure Page

LIST OF TABLES

CHAPTER 1

INTRODUCTION

1.1 Purpose of Study

1.1.1 Mudrock Research

Mudrocks are a very common rock type in almost all sedimentary environments. According to Blatt's studies (1970 and 1985), mudrocks make up approximately 65% of the stratigraphic column of continental blocks and are three times more abundant than sandstone sediments. It is also reported that mudrocks preserve large portions of the earth's stratigraphic history (Schieber and Zimmerle, 1998). While mudrocks make up the majority of continental blocks, they are perhaps under-represented in the geologic literature. There are several possible reasons for the lack of research into mudrocks, including 1) their fine-grained size, which make them difficult to study directly in the field, and 2) difficulties in understanding mineralogical composition made with mineralogical and/or provenance studies very challenging. Though, the main reason why mudrocks were not as pursued by researchers of the past may be due to the fact that mudrocks were not considered to be possible reservoir rock. An increased interest in mudrock studies is due to the recognition of these rocks as potentially valuable hydrocarbon reservoir rocks. Mudrocks commonly form both the source and seal rock to unconventional petroleum systems, and in some cases represent the reservoir itself (Schieber and Zimmerle, 1998; Aplin et al., 1999; Slatt, 2002), as is the case for the Barnett Formation (Hill et al., 2007).

Potter et al. (1980) highlighted the importance of geological studies of mudrocks. Because they represent such a large portion of the stratigraphic record, it is important to understand the processes and history of mudrock deposition. Since then, numerous scientists began contributing to the complex understanding of mudrock research by way of multiple

disciplines: origin of sediments, depositional processes, geochemistry, diagenesis, etc. (Schieber, 1990; Bennett et al., 1991; Zimmerle, 1991; Leithold, 1993, 1994; MacQuaker and Gawthorpe, 1993; Arthur and Sageman, 1994).

1.2 Previous Research

1.2.1 Geochemistry and Methods Used

The geochemical studies of mudrocks have traditionally focused on their redox-sensitive trace metals, iron-sulfur-organic carbon relationships, and stable isotope methods that involve organic carbon (Dean and Arthur, 1989; Jones and Manning, 1994; Crusius et al., 1996; Morford and Emerson, 1999; Rowe et al., 2008; Algeo and Rowe, 2012). It is these relationships that allow geoscientists to deduce important paleoenvironmental data of the past.

The analysis of trace metals that are especially sensitive to redox reactions are specifically helpful to understand the relationships between mudrocks and the chemistry of the overlying water as well as basin hydrography during the time of deposition. According to Vine and Tourtelot (1970), if trace metal enrichment occurs contemporaneously with deposition, oceanographic parameters should exist and therefore be preserved accordingly. Following these assumptions, trace metals can be used to determine bottom-water oxygen conditions in the sediments, overlying water column (Calvert and Pedersen, 1993; Arthur and Sageman, 1994; Piper, 1994; Crusius et al., 1996; Tribovillard et al., 2006; Algeo and Maynard, 2008), and aid in the assessment of basin restriction and deep-water renewal rates (Figure 1.1).

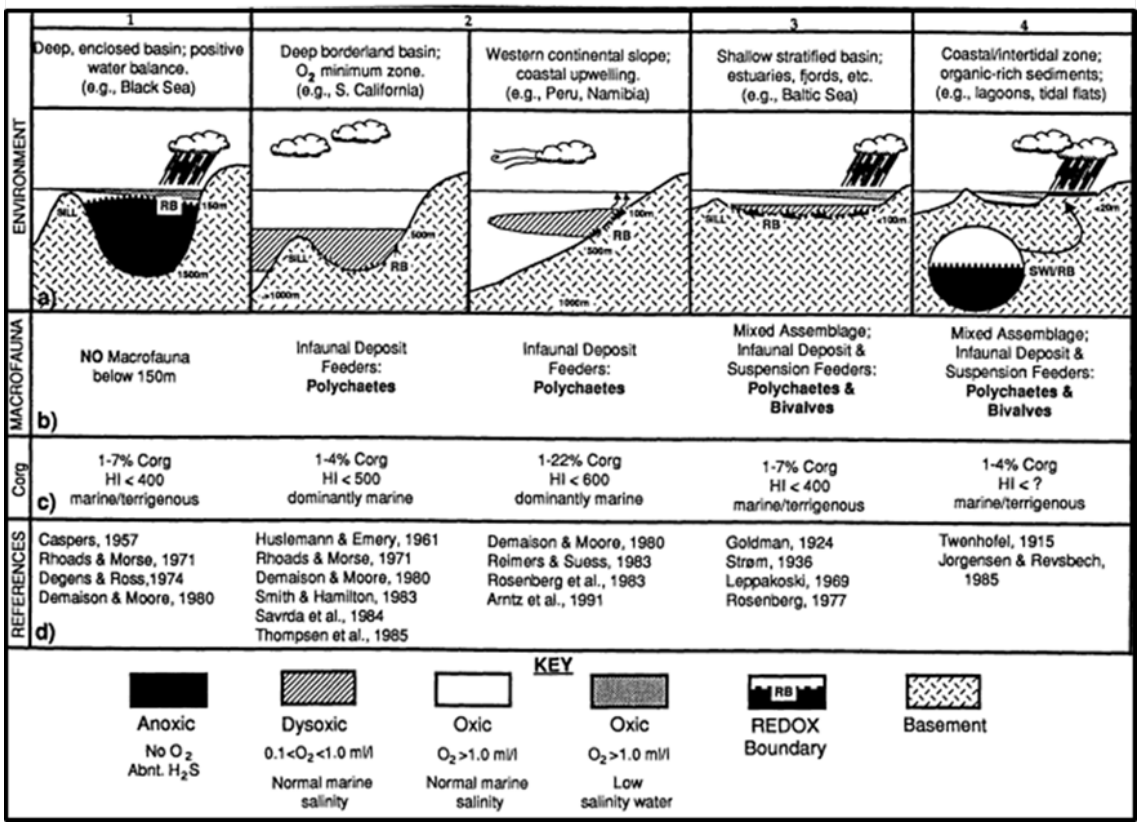

Figure 1.1 Representation of organic matter accumulation in modern marine environments: a) ideal basin and bathymetry, water mass distribution, dominant position of redox boundary (RB), and prevalent climate (rain cloud indicated precipitation > evaporation; cloud streamers indicate offshore winds); b) predominant macrofauna reported from oxygen deficient strata; c) characteristics of organic matter within each environment; d) key references for each environment. (Modified from Arthur and Sageman,1994).

When interpreting bottom-water oxygenation levels, trace metals become enriched or depleted relative to the concentration found in the average gray shale, as defined by Wedephol (1971, 1991) and Tribovillard et al. (2006). Multiple redox-sensitive trace metals may be used in order to evaluate paleo-redox conditions, however the most widely accepted trace metals used for analyses are molybdenum, vanadium, and uranium (Piper, 1994; Crusius et al.1996, Rimmer et al.; 2004; Tribovillard et al., 2006, Algeo and Tribovillard, 2009).

According to Algeo and Lyons (2006), understanding the specific relationship between molybdenum (Mo) and total organic carbon (TOC) can aid in the understanding of hydrographic changes that occurred within basins of both the past and present. Such relationships are useful in understanding the anoxic marine conditions that sediments were subjected to throughout depositional and burial time (Algeo and Lyons, 2006; Algeo et al, 2007; Rowe et al., 2008; Algeo and Rowe, 2011). By creating a cross-plot of Mo(ppm) with total organic carbon (%TOC) and evaluating the slope of the regression line, one may also determine the degree of sub-pycnocnoclinal water mass restriction within the basin as seen in figure 1.2 (Algeo and Lyons, 2006). Such data, used in conjunction with trace-metal covariation, can aid in the understanding of deepwater renewal times.

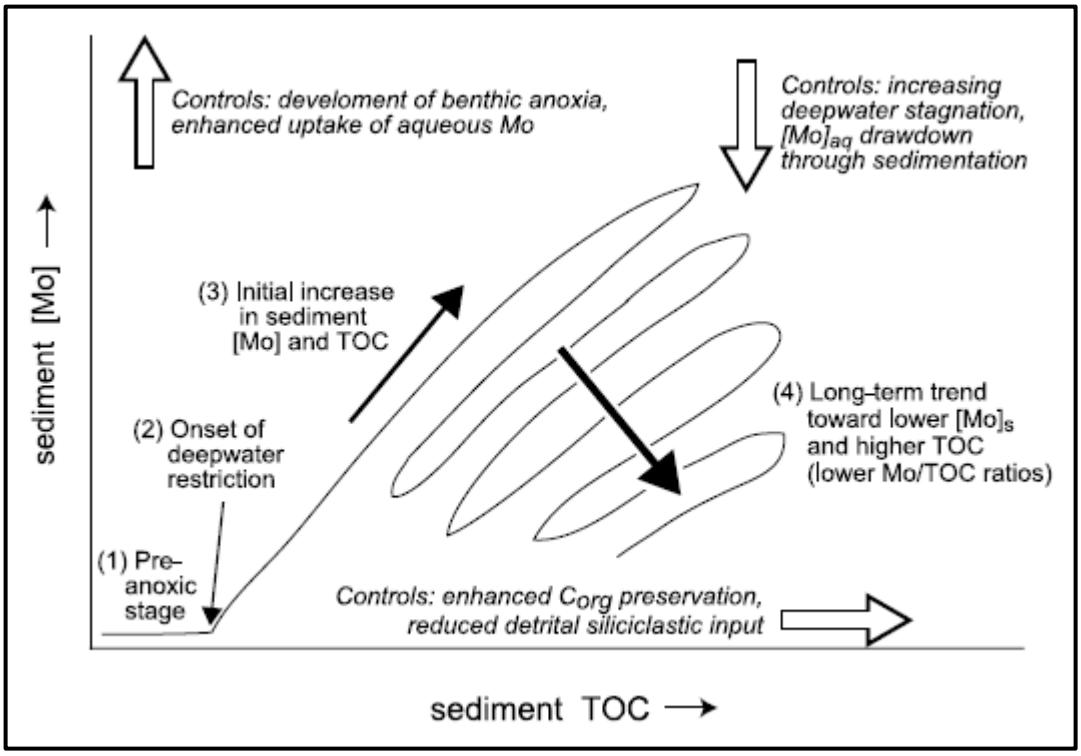

Figure 1.2. General patterns of Mo/TOC covariation associated with deepwater renewal time in silled anoxic basins (Modified from Agleo and Lyons, 2006).

Relationships between iron, sulfur, and carbon have been utilized in order to understand certain paleoceanopraphic properties. Such properties include the distinguishable traits separating normal marine, freshwater, and euxinic conditions from one another, elemental limitations to the formation of pyrite, as well as size distribution of pyrite framboids as paleo-redox condition indicators (Berner and Raiswell, 1983; Raiswell et al., 1988; Wilkin et al, 1996; Wilkin et al., 1997). Such works have laid the foundation to understand the concentrations and inter-relationships of these elements that can be utilized as environmental indicators.

Another approach to understanding paleoenvironments, paleoclimates, as well as provenance is the analysis of stable isotope ratios of carbon and nitrogen ($\delta^{13}C$, $\delta^{15}N$) (Meyers, 1994; Meyers, 1997; Twichell et al., 2002; Meyers et al., 2006). According Meyers and Eadie (1993), changes in $\delta^{13}C$ values during burial are not substantially different from their original algal values. Therefore, $\delta^{13}C$ measurements of shale cores can be utilized to estimate organic matter sourcing.

1.2.2 Geochemical Studies of the Barnett Formation

Due to prolific amounts of natural gas and oil production, previous geological research of the Barnett Formation within the Fort Worth Basin is abundant. Within the past two decades, geochemical analyses have been included in hydrocarbon research (Montgomery et al., 2005; Hill et al., 2007; Pollastro et al., 2007;Jarvie et al., 2007; Maiz, 2007; Rowe et al., 2008; Rodriguez and Philp, 2010). Most of these studies have concentrated on the Newark East Field, with the primary focus being organic chemistry analyses. Research undertaken by Rowe (Bureau of Economic Geology; Austin, TX) and his graduate students at the University of Texas at Arlington, has been completed in attempt to reconstruct the paleoceanography and inorganic geochemistry of both the Fort Worth and Delaware basins during the Cretaceous and Carboniferous periods (Rowe et al., 2008; Rowe et al., 2009; Hoelke, 2011; Hughes et al., 2011). The purpose of these studies are to extend the geochemical understandings of these

basins to their northern most extents, as well as assist in building a more detailed geologic description of the Fort Worth Basin during the Cretaceous and Carboniferous time periods (Cortez, 2012).

1.3 Geologic Information

1.3.1 Geographic Setting of the Fort Worth Basin

The Fort Worth Basin (FWB) encircles approximately 15,000 mi^2 (38,100 km^2) in North-Central Texas (Figure 1.3) (Pollastro et al., 2007). It lies along the paleo Ouachita fold-thrust belt front with a length of approximately 200 miles, and varies in width from approximately 100 miles in the north (Tarrant County) to only a few miles in the south (Llano uplift). The structural margins of the FWB include the Red River and Muenster arches in the North and northeast. The Muenster arch ultimately bends toward the south and parallels the Ouachita thrust front. It is the Ouachita fold-thrust belt that acts as the eastern boundary to the basin. The Llano uplift and Lampasas arch, both, act as the southern boundary of the FWB, and the Bend arch represents the westernmost hinge line. These are the conventionally defined margins of the FWB (Montgomery et al., 2005; Pollastro et al., 2007). However, a wire-line-log study completed by Loucks and Ruppel (2007) suggests the Barnett Formation strata extend further west than the Bend arch prior to complete erosion.

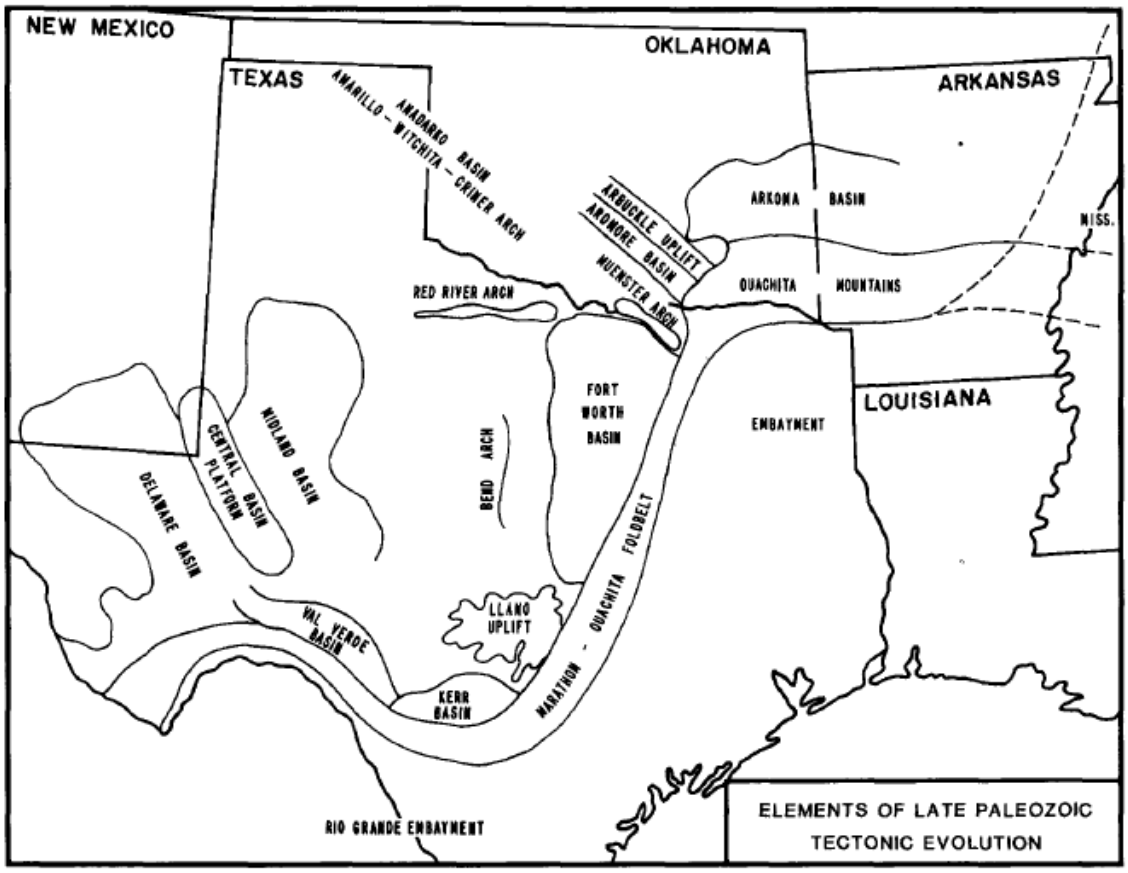

Figure 1.3 Structural elements present during the late Paleozoic (Modified from Walper, 1982).

The Fort Worth Basin axis trends approximately northeast to southwest (Thompson, 1988; Pollastro, 2007). It progressively shifted from west to northwest during the early-middle Pennsylvanian due to movement along the Ouachita fold-thrust belt (Tai, 1979; Walper, 1982; Pollastro, 2007). The basin structure is asymmetric toward the east and northeast along the margins of both the Muenster arch and Ouachita fold-thrust belt. Due to the asymmetrical shape of the Fort Worth foreland basin, Barnett strata thicken toward the northeast along the Muenster Arch and thins progressively southward where it is absent across both the Llano Uplift and Bend Arch (Figure 1.4).

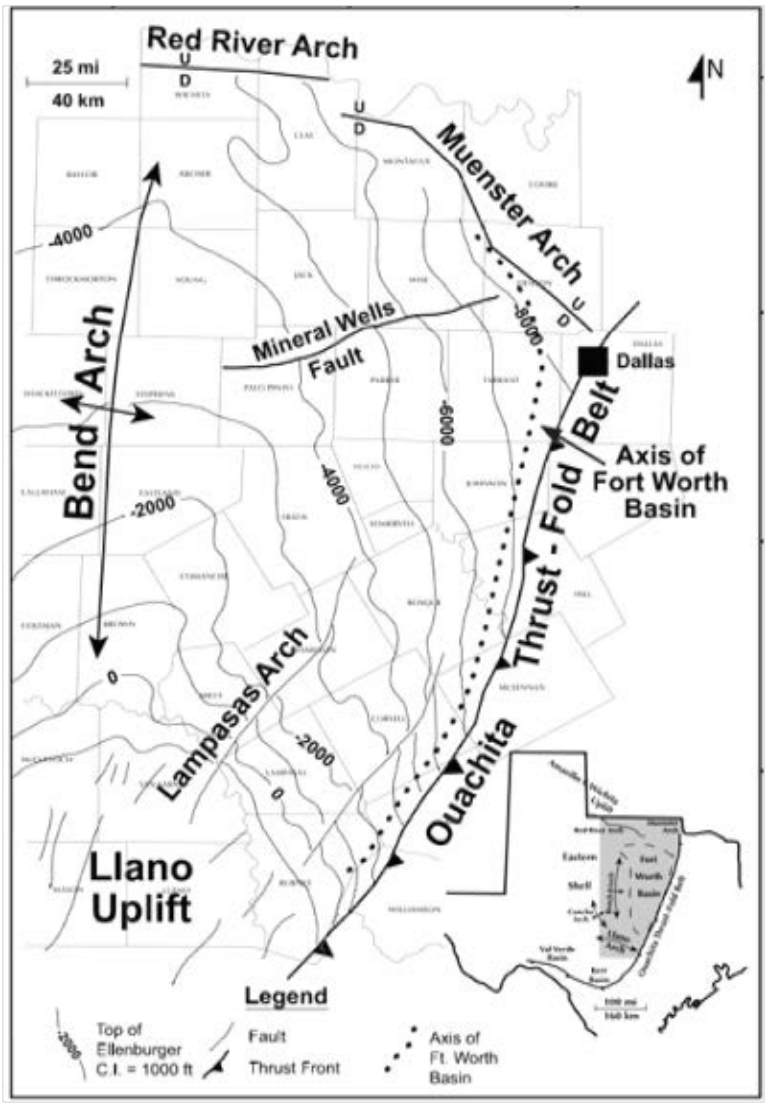

Figure 1.4. Regional setting and structure contour map of the Fort Worth Basin. Contours represent top of the Ordovician Ellenburger Group (C.I. = 1000 ft.). The Barnett Formation is believed to follow same contours (Montgomery et al., 2005).

1.3.2 Global Tectonics and Structural Geology

During the late Paleozoic era (~300 mya), along the eastern margin of present day North America, the supercontinent Pangea was forming as a result of the collision of Laurussia with Gondwana (Figure 1.5). As a result, the Ouachita fold-thrust belt was formed along the

southern margin of the present-day North American continent (Walper, 1982; Thompson, 1988; Pollastro et al., 2007). Due to the structural deformation that occured during such deformation, multiple foreland basins were created along the leading edge of the Laurussian paleocontinent. The Fort Worth Basin is one of the many foreland basins that were created during this time (Arbenz, 1989; Loucks and Ruppel, 2007).

By mid-to-late Mississippian time, during Barnett Shale deposition, the FWB was bordered by the Chappel carbonate shelf in the west and the Caballos Arkansas island arch system in the east (Blakey, 2005; Loucks and Ruppel, 2007). Later, throughout the early and middle Pennsylvanian period, the Ouachita fold belt slowly became a positive feature (Tai, 1979). This uplift caused the Bend arch in the West to tilt west-northwest and ultimately assisted in formation of the modern wedge-shape structure of the basin that is preserved today. According to earlier FWB structure publications, the Bend arch is a flexural high that formed without active uplift, and today represents the westernmost hingeline of the basin (Walper, 1977; 1982; Tai, 1979). It is this movement that also created the Midland Basin to the west (Walper, 1977, 1982; Tai, 1979.). As a result, the Barnett Formation thickens toward the north and northeast adjacent to the Muenster arch, and thins toward the south and southwest against the Llano uplift (Figure 1.6) (Loucks and Ruppel, 2007; Pollastro et al., 2007).

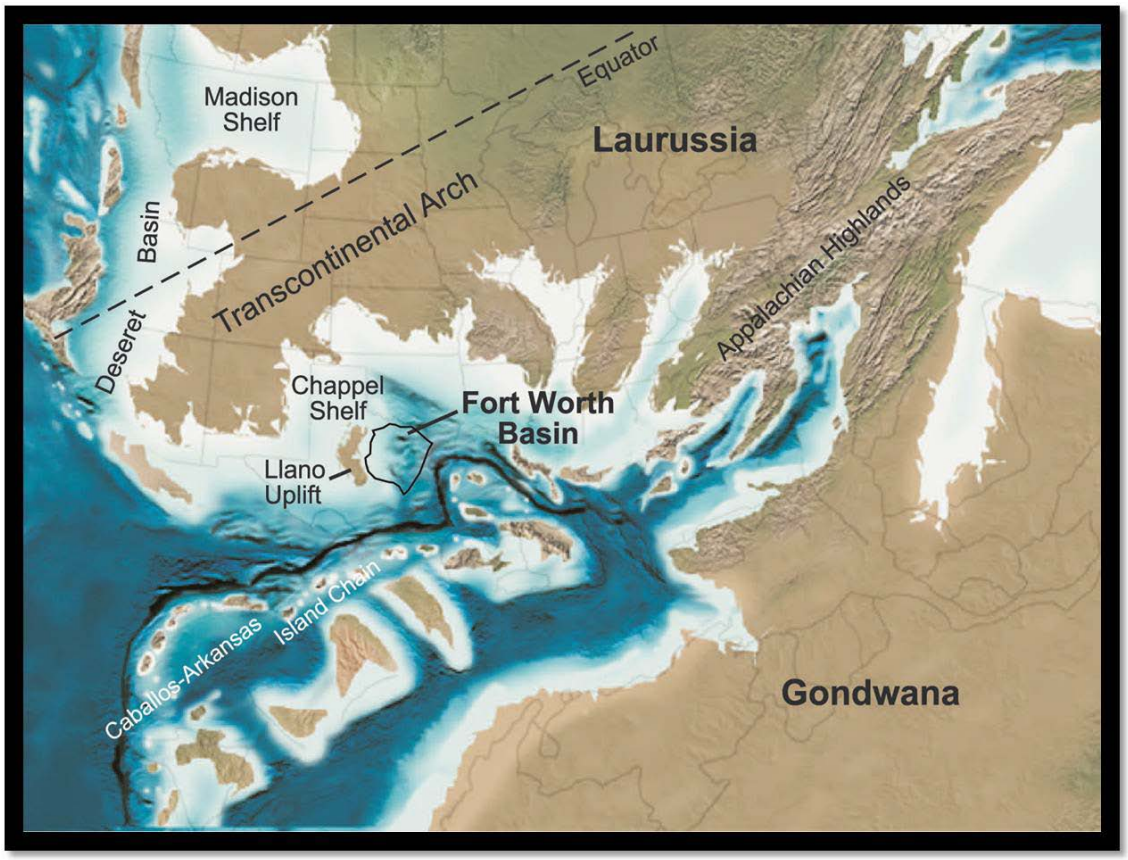

Figure 1.5 Global tectonic map of North America depicting the collision of Gondwana with Laurussia during the late Mississippian (modified plate reconstruction by Blakey, 2005).

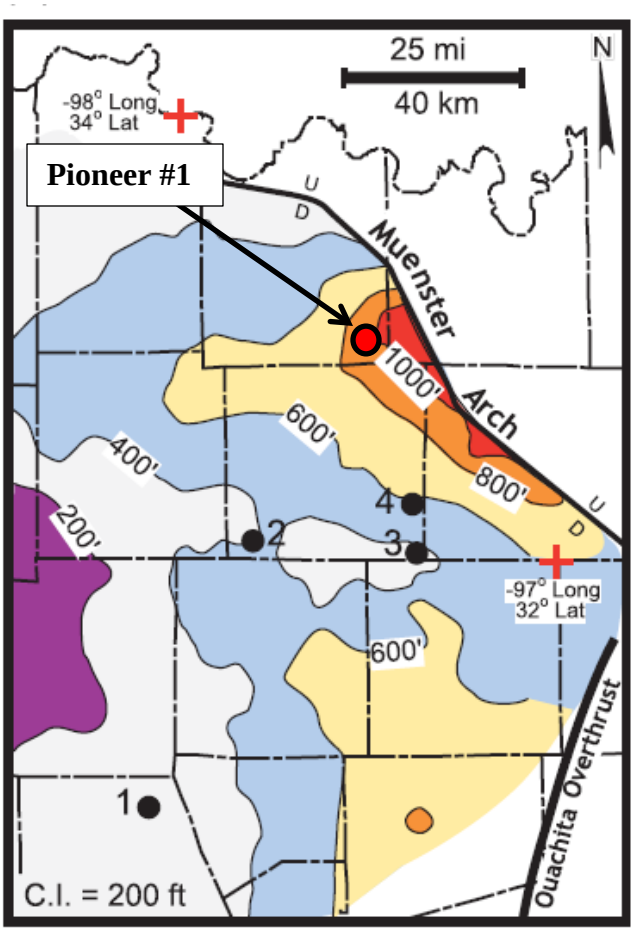

Figure 1.6 Isopach map of total Barnett interval based on wire-line log correlations. Red circle indicated location of Pioneer #1 well (Modified from Loucks and Ruppel, 2007).

1.3.3 Fort Worth Basin Stratigraphy

The Barnett Formation was established as a lithologic unit by Plummer and Moore (1922) based on outcrops located in San Saba County, Texas (Kier et al., 1979). Most Barnett strata unconformably lie above the Middle Ordovician Ellenburger group, however in the western-most extents of the basin, the Barnett sediments unconformably overlie the Lower Mississippian Chappel Limestone and in the North and northeast portions of the FWB the Upper Ordovician Viola-Simpson carbonates. Within the bounds of the FWB, this disconformity is represented by a locally massive pyrite layer (Boardman et al., 2012). Elsewhere, it may be identified as a red paleosol atop the Chappel Limestone. The Barnett Formation is conformably

overlain by the Pennsylvanian Marble Falls Formation throughout the basin (Figure 1.7-a) (Loucks and Ruppel, 2007).

Within the study area, the Barnett Formation is divided into upper and lower Barnett members, due to the presence of the intervening Forestburg Limestone, a carbonate-rich wedge (Loucks and Ruppel, 2007) (Figure 1.7-b) . Much of the Barnett Shale consists of dark, organic-rich, mudrock that is often-times barren of benthic taxa. However, recently published research by Boardman and others (2012), suggests that the strata actually contain pelagic taxa as well as other benthic biota (e.g. bivalves and brachiopods).

The most current and widely accepted interpretation of Barnett Formation deposition is that it occurred during a second order highstand transgression from the Osagean to Chesterian stage (~ 345 to 320 mya)(Ross and Ross, 1987). Loucks and Ruppel (2007) suggest a deep water depositional model (Figure1.8) varying between euxinic and dysaeobic conditions with carbonate shoals and mounds along the Muenster Arch, hemipelagic mud plumes and turbidity flows, as well as upwelling zones. They suggest that sedimentation to the basin occurred by way of 1) suspension settling (e.g. radiolarians and forams), or 2) density currents. However, opposing research suggests the Barnett Formation was deposited under normal marine conditions within the southern Oklahoma Basin, prior to the formation of the Fort Worth Basin (Henry, 1982; Thompson et al., 1988). Therefore, a primary purpose of this thesis is to differentiate between the two models based upon geochemical results and analysis and decide which model is the more likely, or neither.

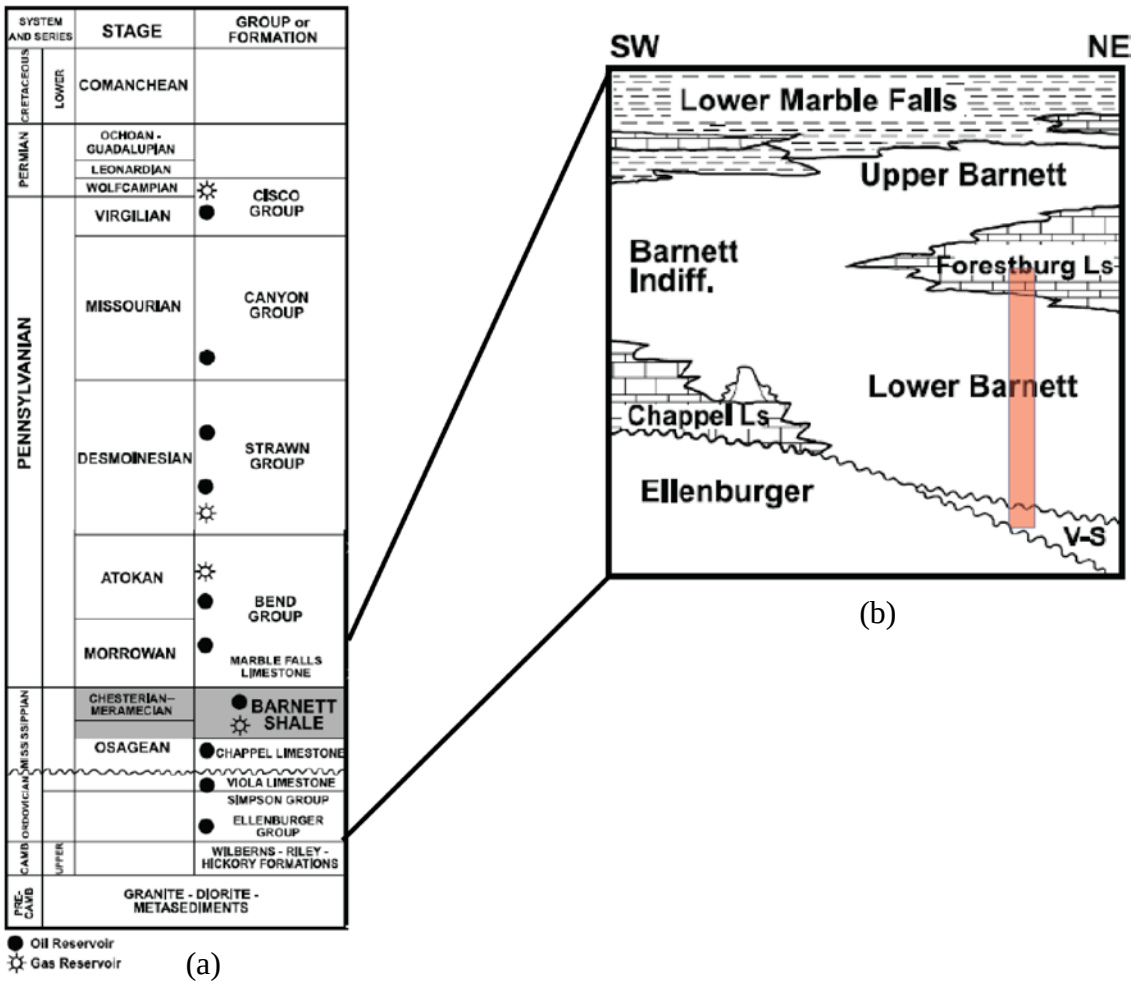

Figure 1.7 Fort Worth Basin stratigraphy: (a) Generalized stratigraphic column of Fort Worth Basin rocks. (b) Expanded section shows more detailed interpretation of Mississippian stratigraphy. Red shading indicates formations contained in Pioneer #1 core. (V-S = Viola/Simpson interval) (Modified from Montgomery et al., 2005).

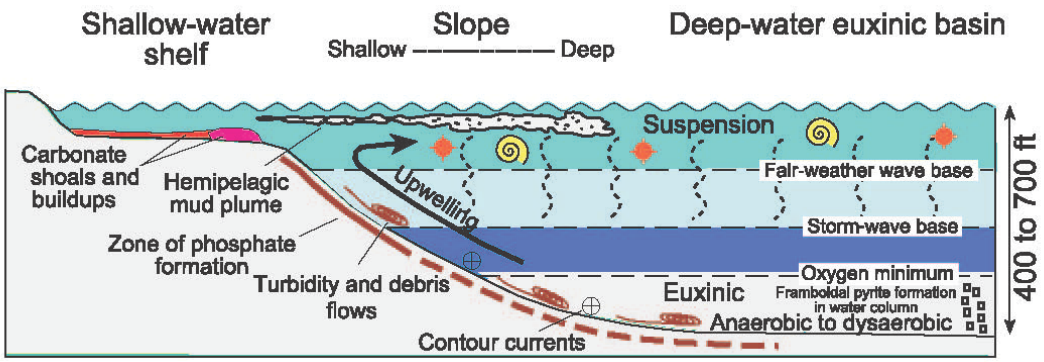

Figure 1.8 Deep-water depositional model of the Barnett Formation (Loucks and Ruppel, 2007).

1.4 Research Objective

1.4.1 Research Objective

The purpose of this study is to construct a further evaluation of both the chemostratigraphy and paleoceanography of the Barnett Formation in the northern end of the Fort Worth Basin in North-Central Texas. Major research objectives of this study include: 1) determination of the degree of water restriction within the northern FWB, 2) assessment of the mechanism(s) driving geochemical changes in environmental redox conditions, 3) specify zones of increased organic preservation and accumulation for future hydrocarbon production, 4) creation of chemostratigraphic correlations of geochemical data to well log data.

CHAPTER 2

METHODS

2.1 Core Information

A 647 foot-long drill core, Pioneer #1, from southern Montague County, Texas (Figure 2.1) was slabbed into a 2/3 section and 1/3 section. XRF analyses were completed on the slabbed face of the 2/3 section of the core at 1-foot increments. The core is currently located at Weatherford Core Laboratories, Houston, Texas.

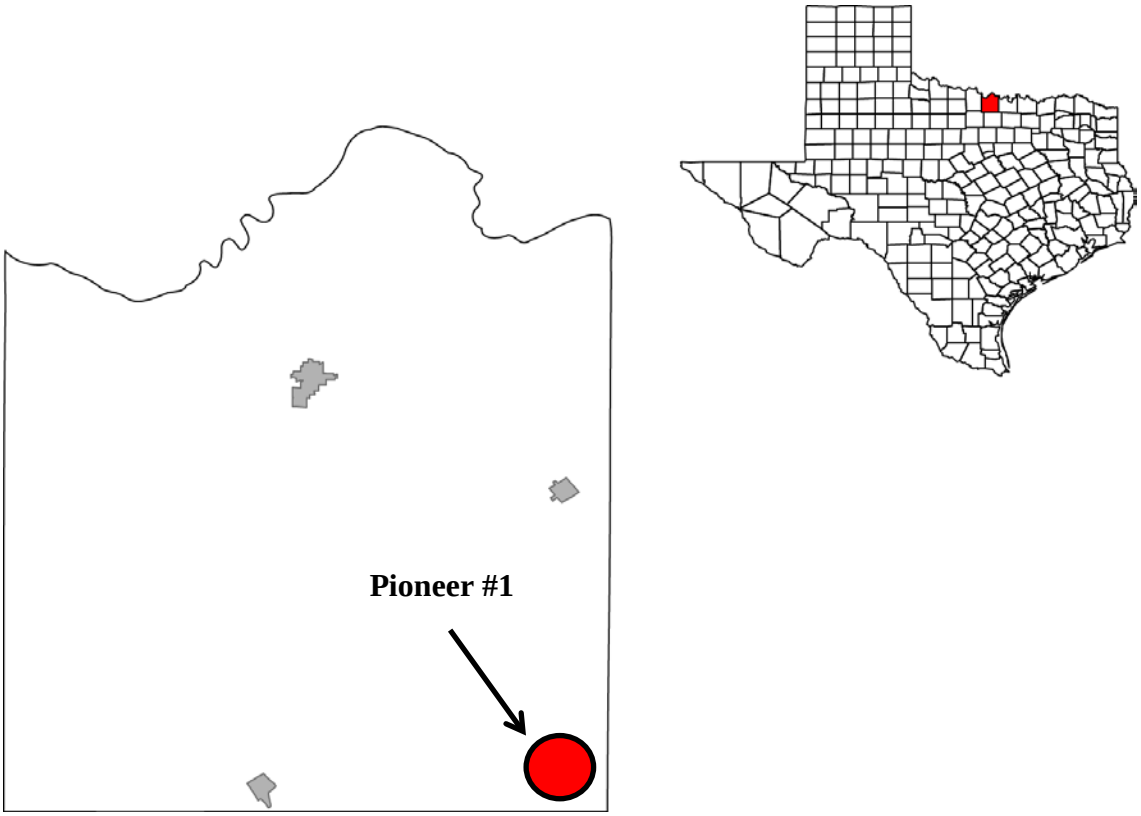

Figure 2.1 Location of Montague County, TX. Location of Pioneer #1 well shaded in red.

2.1.1 Well Logs

Four separate well logs, gamma ray, resistivity, neutron porosity, and density porosity for the Pioneer #1 well were provided by Pioneer Natural Resources. The gamma ray log was used to measure the natural radioactivity in the formation and aids in identifying lithologies and correlating zones. Carbonates and shale-free sandstones generate low gamma ray readings, while clays and other strata rich in potassium, uranium and thorium (e.g. ash layers) produce a higher gamma ray response due to their increase in such radioactive materials. Resistivity logs are used for multiple reasons. They can help determine hydrocarbon-bearing *versus* water-bearing zones, aid in permeability assessment, and determine porosity. The neutron porosity log measured the amount of hydrogen richness within a given formation. This specific log can be used to assess lithologic identification, correlation, and most importantly assess the porosity or total water content of the formation. Lastly, the density porosity log was used to measure the degree of porosity within the formation as well as assist in lithology identification. These logs were integrated with the geochemistry data of this study.

2.2 Energy Dispersive X-ray Fluorescence (ED-XRF) Analysis

2.2.1 ED-XRF Analyis

Core samples were marked prior to ED-XRF analysis at an approximately one-foot (~0.3m) interval. Two Bruker Tracer III-V handheld ED-XRF spectrometers were used to measure metal concentrations in each sample, UTA-1 for trace elements and UTA-2 for major elements. Both instruments were stabilized using a plastic platform. Samples were positioned on the nose of the instrument, directly above the 3 by 4 mm elliptical beam window, and stabilized by using a platform around the nose of the instrument. Measurement sensitivity of the ED-XRF instruments decreases by the inverse square of the distance from the silicon detector (SiPIN), located directly beneath the sampling window. This flat sample surface is needed in

order to optimize measurement consistency. All core samples were analyzed on the slabbed side whenever possible and samples that were unslabbed were given a flat surface for analysis using a Dremel grinding hand tool.

Samples were analyzed for major and trace element concentrations for 180 seconds each. Major element data acquisition, which includes V and Cr measurements, were undertaken using a low-energy, vacuum-pumped instrument setting. Low-energy spectrum acquisition included all elements that emit characteristic x-rays between 1.25 to 7.06 kV. In order to obtain the elements in this range, and allow for backscatter that does not interfere with the elemental peaks of interest, the voltage on the instrument was set to 15kV. Voltage settings on the instruments remained constant for their respective elemental range of interest; however, the current settings vary between instruments due to the variability associated with the manufacturing of the x-ray tube and inter-instrument electronics. For major element data acquisition, the current was set to 35 μA.

Trace element data acquisition required use of the high-energy instrument setting and a Cu-Ti-Al filter in order to greatly reduce the low-energy x-rays from reaching the detector. The UTA-1 instrument voltage was set to 40kV and current at 25 μA in order to detect x-rays between 6.92 and 19.80kV. For further information on energy dispersive X-ray fluorescence techniques and X-ray fluorescence in general, see Rowe et al. 2012.

Figure 2.2 Picture of a Bruker Tracer III-V handheld ED-XRF spectrometer that was utilized for geochemical analysis. Note: 2/3 section of slabbed core sitting atop sptectrometer aperture.

2.2.2 Mudstone Calibration of ED-XRF

Calibrations of the ED-XRF instruments for both major and trace elemental analysis were produced using a suite of ninety-one reference materials. The reference materials include twenty-seven from Devonian-Mississippian Woodford Formation, twenty from the Pennsylvanian Smithwick Formation of Central Texas, sixteen from the Mississippian Barnett Formation of North Central Texas, fifteen from the Late Cretaceous Eagle Ford formation of South Texas, seven from the Devonian-Mississippian Ohio shale, and five international standards (Rowe et al., 2012). There are limits of determination of a method (LDM) for each element, and are provided in Table 3 (Rosseau, 2001).

A specific limitation of the calibration is observed in samples with calcium concentrations higher than ~40%. Under these conditions, the percent aluminum is calculated

to be a negative value. This situation occurs in the Ellenberger and Viola formations, as well as the Forrestberg member. To partially overcome this artifact of the dataset, values for aluminum that are calculated to be negative are assigned a positive value of +0.01%. This, in turn, produces an artifact in the dataset when aluminum is used in the denominator of elemental ratios. For instance, if calcium in 35% and is divided by the assigned value of aluminum (0.01%) the resulting ratio is very high (1750). It should be noted that these values simply denote very high calcium concentrations in the rocks, and that no quantitative significance should be given to them. Fortunately, the newer generation of XRF instruments provides an updated calibration correction to better evaluate aluminum concentrations in high calcium lithologies.

Table 1.1 Lowest Detectable Measurements for XRF Instruments (UTA-1 and UTA-2)

Element	Accepted Value[a]	Instrument 1 (UTA-1)			Instrument 2 (1st UTA-2)		
		Measured Value[b]	σ (n=7)[b]	LDM[c]	Measured Value[b]	σ (n=7)[b]	LDM[c]
Mg (%)	0.67	0.80	0.09	0.17	0.85	0.14	0.28
Al (%)	4.96	5.39	0.14	0.28	5.32	0.11	0.22
Si (%)	32.6	33.7	0.2	0.5	33.1	0.4	0.8
P (%)	0.07	0.05	0.03	0.07	0.09	0.03	0.06
S (%)	3.34	2.18	0.10	0.20	2.27	0.09	0.18
K (%)	2.07	2.31	0.09	0.18	2.22	0.07	0.14
Ca (%)	0.13	0.23	0.03	0.06	0.24	0.02	0.04
Ti (%)	0.23	0.27	0.02	0.04	0.27	0.02	0.03
Mn (%)	0.015	0.012	0.001	0.002	0.013	0.001	0.003
Fe (%)	2.93	2.55	0.06	0.12	2.52	0.06	0.13
Ba (ppm)	2090	1884	376	753	1706	300	600
V (ppm)	928	1114	68	137	1110	80	159
Cr (ppm)	110	98	13	26	106	14	27
Ni (ppm)	130	153	26	52	150	20	40
Cu (ppm)	83	147	20	40	87	12	23
Zn (ppm)	823	844	96	191	880	74	147
Th (ppm)	8.4	9	1	2	9	1	2
Rb (ppm)	122	123	12	25	131	12	25
U (ppm)	18.1	17	6	11	22	4	8
Sr (ppm)	75.5	87	5	10	93	9	18
Y (ppm)	35.4	34	3	5	36	2	4
Zr (ppm)	80.3	95	7	13	96	6	13
Nb (ppm)	9	9	1	2	9	1	2
Mo (ppm)	79	83	4	9	82	3	6

A – Values for major elements from lithium borate-fused disc analysis by WD-XRF at SGS; values for trace elements (ppm) from sodium borate fusion dissolution and analysis by ICP-MS.
B – Average HH-ED-XRF measured values (n = 7) and standard deviations for reference material RTC-W-260, a shale sample from the Devonian Woodford Formation of West Texas.
C – Limit of Determination of a Method (LDM) calculated according to Rousseau

2.3 Additional Geochemical Analysis

2.3.1 Sample Preparation

Samples for additional analyses were collected from most sample locations at approximately one foot intervals along the convex (2/3) side of the slabbed core. A Dremmel hand-tool and Dewalt hand drill were used along with a 0.5 cm tungsten carbide grinding bit and a 3/8 inch carbide tipped drill bit, respectively. Samples were properly labeled and stored in capped plastic vials. The subset of samples used for additional geochemical analysis is provided in Table 1.

TABLE 2.1 Depths with additional geochemical analyses.

Depth	**%TIC**	**%TOC**	**$\delta^{13}C_{org}$**
7770' – 7835'		X	
7836' – 8113'	X	X	X
8114' – 8116'	X		
8117' – 8207'	X	X	X
8208' - 8214'		X	X
8215' – 8270'	X	X	X
8271' – 8349'		X	X

2.3.2 Total Inorganic Carbon (TIC)

Samples were analyzed for their total inorganic carbon (TIC) content utilizing a UIC, Inc. coulometer equipped with a CM5230 acidification module. The UIC, Inc. coulometer has an average unknown standard deviation of less than 0.5 percent (Engleman et al 1985). Samples were weighed out between 2-5 mg and acidified at 70^{o}C with ten percent (10%) phosphoric acid (H_3PO_4). The subset of samples analyzed for TIC are represented in Table 1.

2.3.3 TOC and Carbon Isotopes

Total organic carbon (TOC) and stable isotopic composition of TOC ($\delta^{13}C$) were performed on powdered samples. Samples were weighed into silver capsules between 13 – 18 mg (Costech Analytical, Inc. #41067) and later acidified repeatedly with six percent (6%) sulfurous acid (H_2SO_3) in order to remove all inorganic carbonate phases (Verardo et al., 1990). Samples were analyzed using a Costech 4010 elemental analyzer interfaced with a Thermo Finnigan Conflo IV device to a Thermo Finnigan Delta-V isotopic ratio mass spectrometer (IRMS) located at the University of Texas at Arlington. Isotopic results were reported in parts per mil (‰) relative to V-PDB for $\delta^{13}C_{org}$ with an average standard deviation of 0.11‰ of USGS-40 glutamic acid (IAEA-8573) and 1.07‰ for the TOC of USGS-40. The subset of samples analyzed for TOC and stable isotopic composition of $\delta^{13}C$ are represented in Table 1.

CHAPTER 3

RESULTS

3.1 General Data

3.1.1 X-Ray Fluorescence Data

Cross-plots presented here represent results of x-ray fluorescence spectrometry and other geochemical analyses that were formerly described in Chapter two. All down-core plots have their units displayed in 1) per mil (‰), 2) weight percent (e.g. % Al), or 3) expressed as an enrichment factor (EF). Enrichment factors are used to express elemental ratios that are enhanced within the samples relative to their natural abundance in the average gray shale (Wedepohl 1971, 1991). This approach was used for multiple trace elements within the XRF spectrum. The enrichment factor equation is as follows:

$$EF = (\text{element in ppm/Al in ppm})_{\text{sample}} / (\text{element in ppm/Al in ppm})_{\text{standard}}$$

All graphs of x-ray fluorescence spectrometry plotted relative to core depth have their units displayed in weight percent or parts per mil.

The element aluminum is used to represent the clay (e.g. shale) fraction of the rocks. There are several elements that are considered to represent geochemical proxies and/or fractions of the mudrock sediments. Such proxies are represented in Table 2.

Table 3.1 Major Elements and their mineralogical proxies.

Major Element	**Mineralogy / Proxy**
Silica (Si)	Sio_2 → Quartz $KAl_2(SiO_3ALO_{10})(OH)_2$ → Illite (e.g. clay)
Aluminum (Al)	$KAl_2(SiO_3ALO_{10})(OH)_2$ → Illite (e.g. clay)
Iron (Fe)	$KAl_2(SiO_3ALO_{10})(OH)_2$ → Illite (e.g. clay) FeS_2 → Pyrite Carbonates: Siderite, Ankerite, Dolomite Vivianite
Calcium (Ca)	Carbonates: Siderite, Ankerite, Dolomite $CaCO_3$ → Calcite Phosphates: Apatite, Francolite, Vivianite
Sulfur (S)	FeS_2 → Pyrite $CaSO_4 – 2(H_20)$ → Gypsum
Titanium (Ti)	$KAl_2(SiO_3ALO_{10})(OH)_2$ → Illite (e.g. clay)

Defined units within the Barnett Formation and Viola Limestone Formation suggested in this thesis were created based upon elemental enrichments in calcium, silica, or aluminum (Figure 3.1). Unit B of the lower Lower Barnett was demarcated by its silica enrichment relative to the upper Lower Barnett strata of Unit A and the calcium rich strata of Unit C. Unit A lies above the Ca-rich Barnett Unit C and begins with a high clay zone transitioning into a more calcium rich zone, and capped by a slightly enriched silica zone prior to deposition of the Forestburg Limestone Member. The Viola Limestone Formation was separated into two separate units due to their silica or calcium enrichments relative to one another.

3.1.2 Well Logs and Geochemistry

Geochemical results from the XRF analysis were also plotted versus depth and placed next to the Pioneer #1 well logs, at their respective depths. Results define multiple zones of various elemental enrichments, and are noted with separate colors (Red = silica rich, Gray = clay rich, and Blue = calcite rich. These separate zones are also represented in the legend.

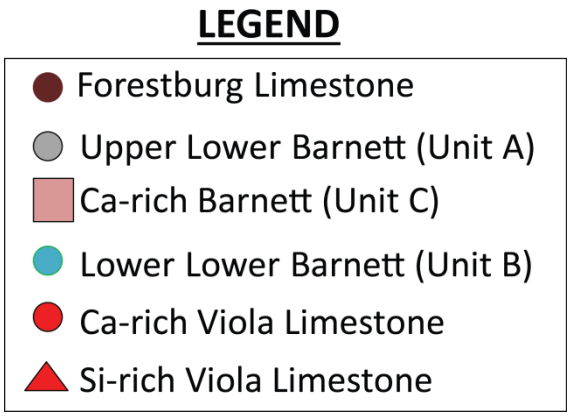

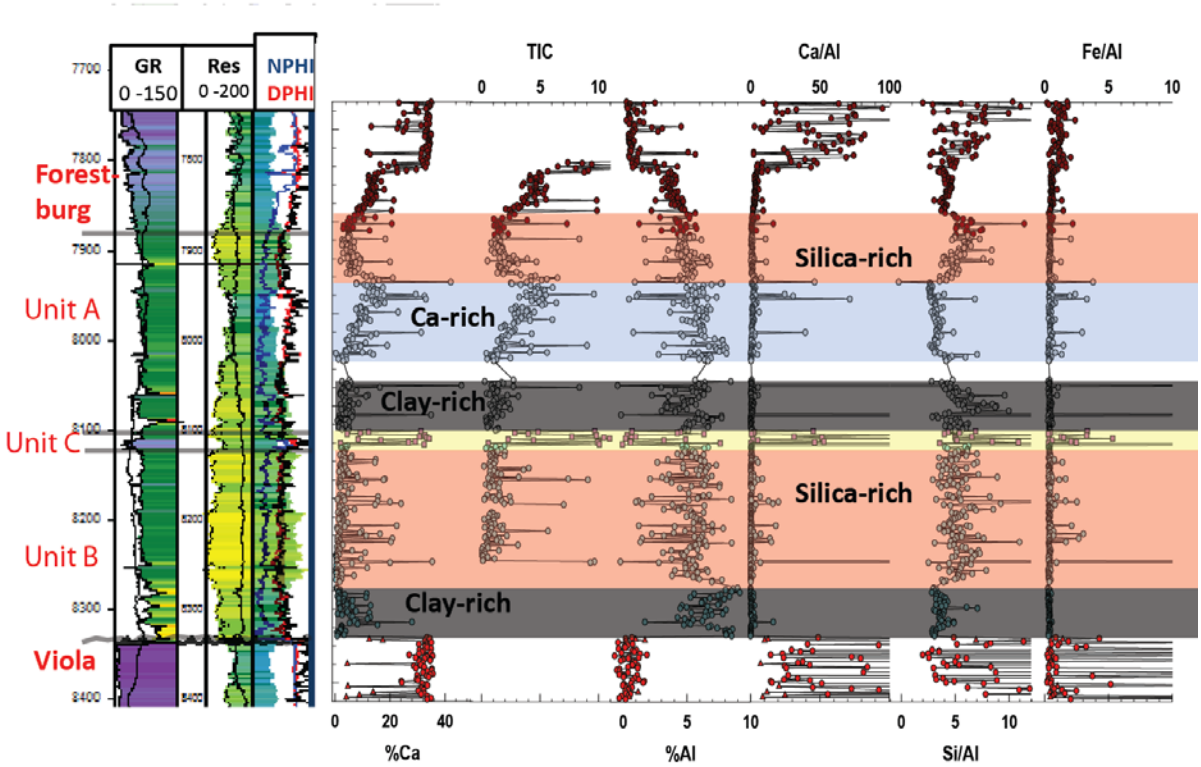

Figure 3.1 Pioneer #1 well logs versus chemostratigraphy. Logs presented (from left to right): total gamma ray, resistivity, neutron porosity, density porosity, %Ca, TIC, %Al, Ca/Al, Si/Al, and Fe/Al.

3.1.3 Bulk Mineralogy

The cross-plot of %K *versus* %Al (Figure 3.2 (a)) demonstrates two separate trend lines. Samples from Unit B establish a larger presence of potassium, while samples from Unit A exhibit slightly lower amounts of potassium. The %Ti *versus* %Al (Figure 3.2 (b)) cross-plot reveals a strong linear trend. Samples from both the Forestburg Member and Viola Limestone Formation contain the lowest levels of both titanium and aluminum, while samples from both Units A and B represent a positive trend.

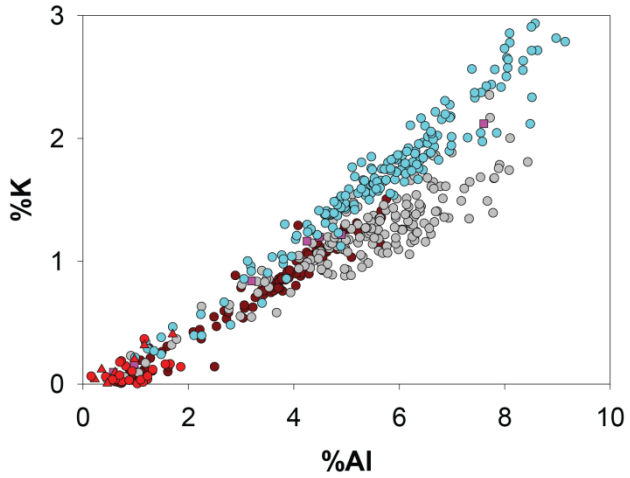

(a)

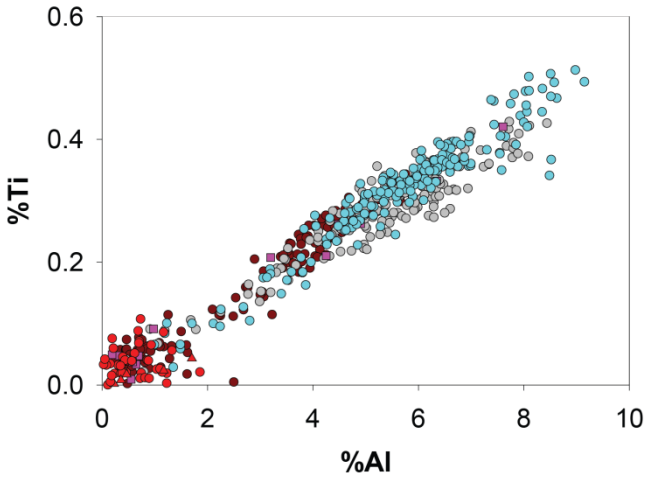

(b)

Figure 3.2 Cross-plots of a) Potassium (%) *versus* aluminum (%); b) titanium (%) *versus* aluminum for Pioneer #1 core.

A cross-plot of %Fe *versus* %Al (Figure 3.3) reveals a sub-linear trend between the two elements. Most samples from both Units A and B reveal a positive trend. However, multiple samples within these units plot above the general trend illustrating an enrichment of iron relative to aluminum.

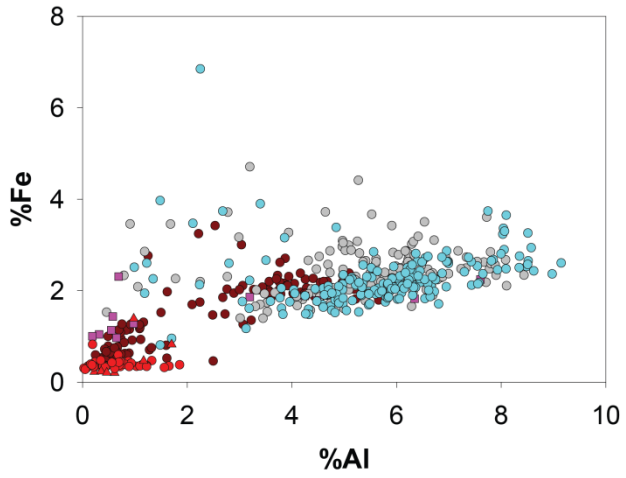

Figure 3.3 Cross-plot of iron *versus* aluminum (%) for the Pioneer #1 well.

3.1.4 Carbonate Mineralogy

A cross-plot of %Ca *versus* %P (Figure 3.4) is used to assess the relationship of phosphorous with the carbonate phase. Samples from the Forestburg Member, Viola Limestone, and Unit C demonstrate the highest amounts of %Ca, while samples from unit B demonstrate a low concentration of %Ca and variable amounts of %P. Samples from Unit A display variable amounts of both %Ca and %P.

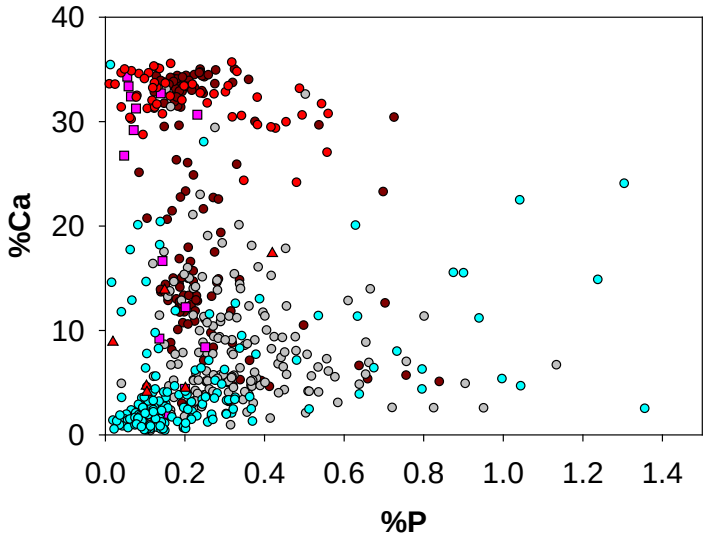

Figure 3.4 Cross-plot of calcium (%) *versus* phosphorous (%) for Pioneer #1 core.

A cross-plot of %Mg *versus* %Ca (Figure 3.5) is used to illustrate the relationship of magnesium with the carbonate phase. Most samples from Unit A and B display a linear trend; however a number of these samples plot above the general trend indicating a greater percentage of magnesium is present in those samples. Samples from the Forestburg Member and Viola Limestone Formation demonstrate a high percentage of calcium and variable amounts of magnesium throughout, as well as demonstrating the highest levels of magnesium.

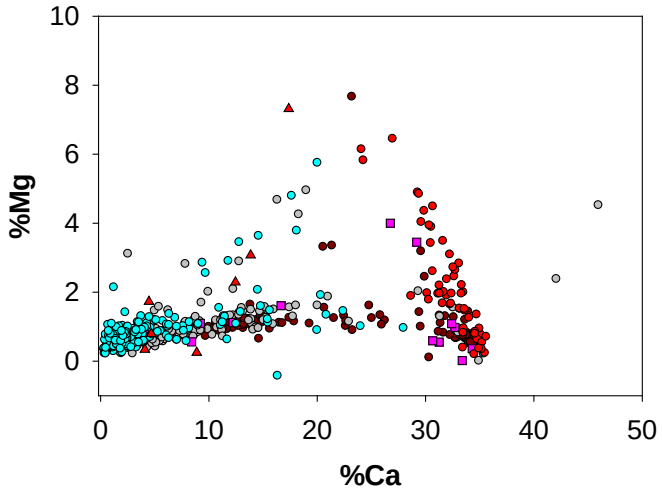

Figure 3.5 Cross-plot of magnesium (%) *versus* calcium (%) for Pioneer #1 core.

3.1.5 Iron Mineralogy

Multiple cross-plots of Fe/Al versus other elements (Figures 3.6 a, b, and c) are used to interpret iron's relationship to other bulk mineralogical phases, while normalizing iron to the clay fraction. The cross-plot of Fe/Al *versus* %TIC (Figure 3.6 (a)) reveals a sub-linear trend with most samples; however multiple samples from Unit B and Unit A plot above the trend indicating an enrichment of iron relative to the carbonate phase in these zones. No trend is seen in the Fe/Al *versus* %Mg cross-plot (Figure 3.6 (b)), though a trend is present between Fe/Al versus %S (Figure 3.6 (c)). Most samples from both Unit A and Unit B depict high amounts of sulfur present relative to iron, while samples from both the Forestburg Member and Viola Limestone Formation have relatively low amounts of both iron and sulfur.

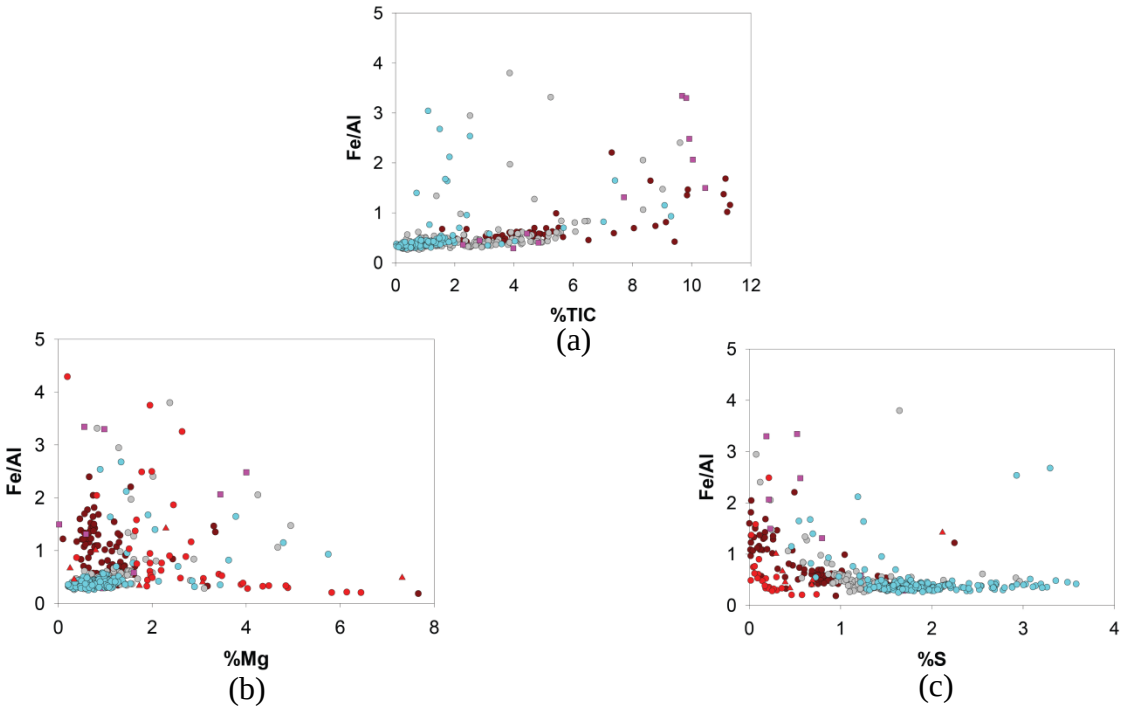

Figure 3.6 Fe/Al cross-plots: a) cross-plot of Fe/Al *versus* TIC (%); b) cross-plot of Fe/Al *versus* magnesium (%); c) cross-plot of Fe/Al *versus* sulfur (%).

3.1.6 TIC Data

All total inorganic carbon data are presented in weight percent (e.g. % TIC). Such plots include both %TIC *versus* depth as well as multiple cross-plots. Total inorganic carbon data are used to assess the presence of carbonate and non-carbonate phases present with each respective mineral. Data presented here are mostly representative of the carbonate fraction.

The down-core plot of %TIC *versus* depth (Figure 3.7) reveals its highest values within both the Forestburg Limestone (dark red) and unit C (pink) intervals, with a maximum of 12% TIC. The samples of unit B (grey) represent the highest degree of variability within the core. Samples ranging from 7840' – 7950' and 7991' – 8130' exhibit an overall decrease in %TIC, while samples ranging from 7951' – 7990' represent a positive trend. Unit A samples (cyan) remain stable at >2% TIC with a few ranging up to 10%. Such variability indicates episodes of

calcium-rich sediment deposition within the basin, possibly due to density currents from the adjacent shelf.

Cross-plots of %TIC with various elements are also presented here (Figures 3.8 a, b, and c). The %TIC *versus* %Ca cross-plot displays a strong linear relationship. Multiple data points lie above the “calcite” line and suggest that calcium may be present in other mineral phases. Elements, %Ca, %Fe, and %Mg all show a sub-linear trend with %TIC. Data points falling above or below the trend line suggest an enrichment or depletion in other mineral forms, respectively.

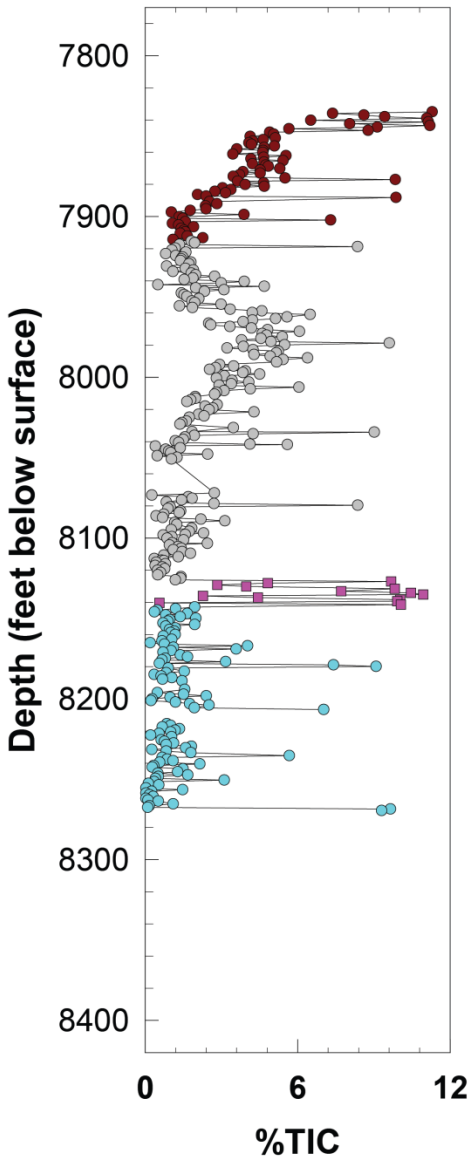

Figure 3.7 Total inorganic carbon (%) versus depth for Pioneer #1 core.

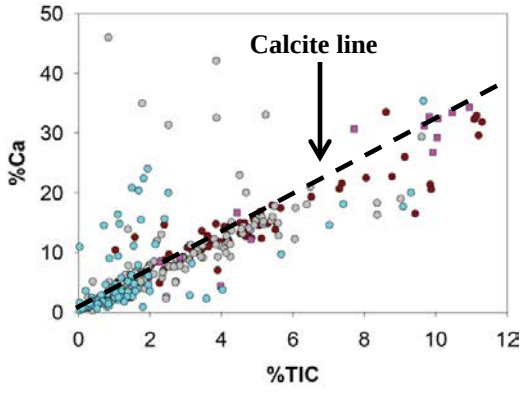

(a)

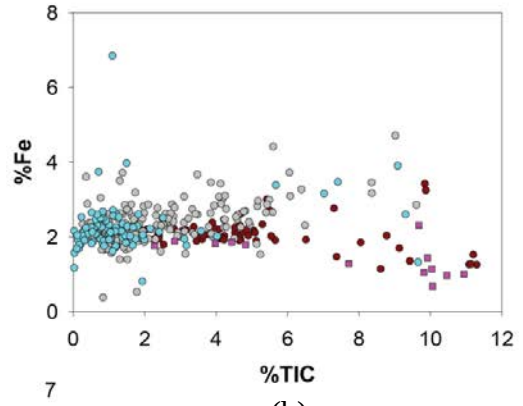

(b)

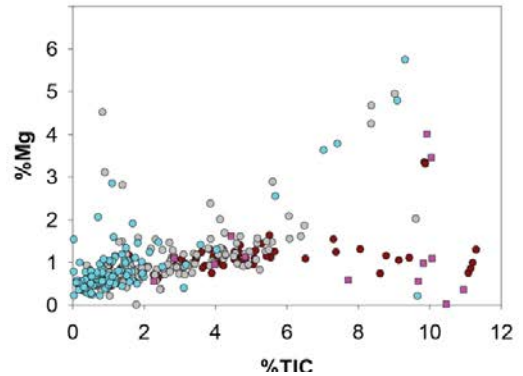

(c)

Figure(s) 3.8 Total inorganic carbon *versus* a) calcium, b) iron, and c) magnesium for the Pioneer #1 core.

3.1.7 TOC Data and Organic Carbon Isotopes ($\delta^{13}C_{org}$)

TOC (total organic carbon) measurements are presented in total weight percent (e.g. % TOC) excluding the TOC-S-Fe ternary plots which represent an enrichment that has been normalized. Figure 3.9 exhibits an overall increase in %TOC throughout unit A samples with an increase in variability from footages 8070' to 8120'. An abrupt decrease is seen within the unit C, followed by relative consistency for all unit B samples, averaging ~5% TOC. Samples representing the lowest % TOC lie within both the Forestburg Limestone Member and unit C. [Average %TOC for the Pioneer #1 core is 3.2%, and ranges from 0.30% to 11%.]

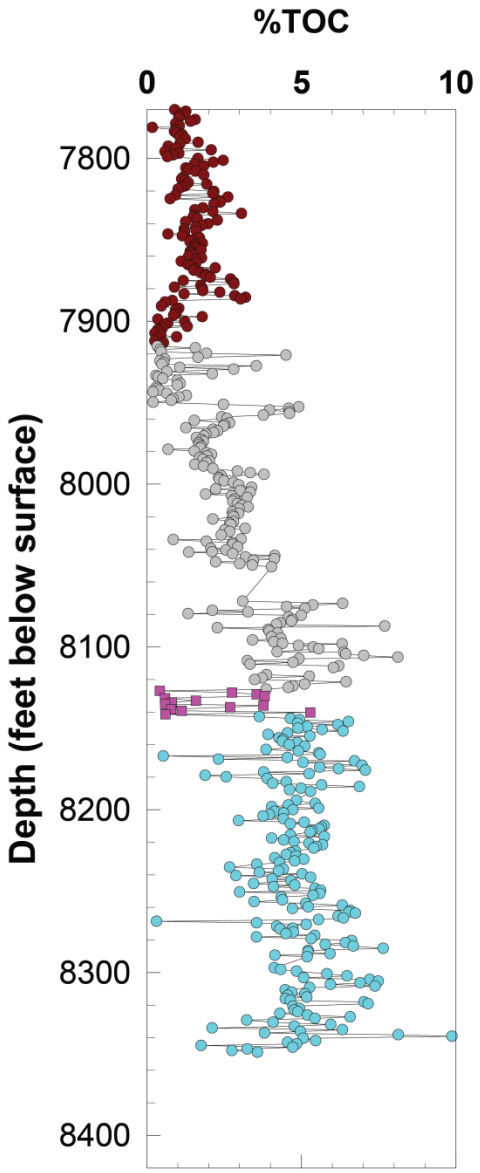

Figure 3.9 Total organic carbon (%) *versus* depth for Pioneer #1 core.

Organic carbon isotope ($\delta^{13}C_{org}$) measurements are presented as per mil (‰). Results range from ~ -25‰ to 32‰ with an average of -29.3‰ (Figure 3.10). Results from the Pioneer #1 well demonstrate a progressive decrease in the $\delta^{13}C_{org}$ isotope down-core.

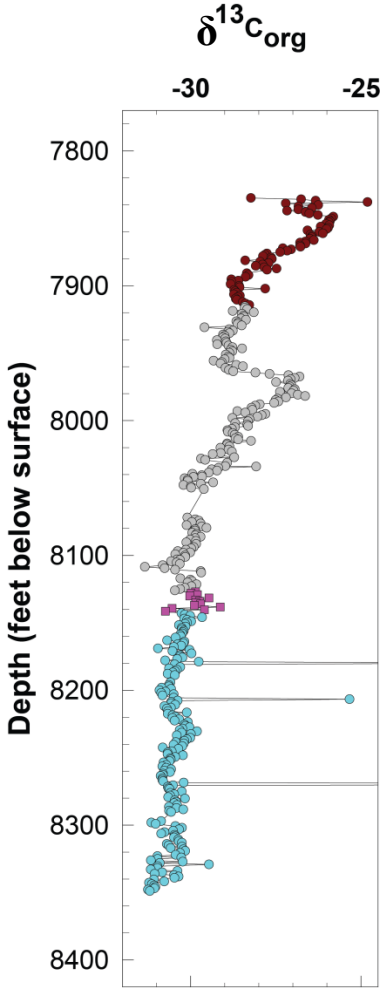

Figure 3.10 $\delta^{13}C_{org}$ *versus* depth for Pioneer #1 core.

3.2 Integrated Data

3.2.1 Silica, Aluminum, and Calcium Oxide Ternary Diagram and Cross-plots

A calcium oxide (CaO), alumina (Al_2O_3), and silica (SiO_2) ternary diagram is used to compare the composition of the samples against that of the average gray shale, as defined by Wedepohl (1971, 1999). These diagrams were created using normalized data (e.g. normalized

weight percentages of 2(CaO), 5(Al_2O_3), and SiO_2). Calcium oxide (CaO), alumina (Al_2O_3), and silica (SiO_2) represent the quartz, calcium, and clay phases of the lithologic system. Such figures allow one to visualize the major constituents and their relative enrichments within the system. Results from the Pioneer #1 core (Figure 3.11) illustrate a variable amount of quartz and calcite dilution of the "average gray shale"; however, several grey, green, and red (triangles) samples define a calcite-dilution trend toward the calcite end-member composition. This trend is indicative of a relative increase in calcite in these particular zones. Multiple samples also demonstrate silica enrichments as they are plotted off the line toward the silica end member.

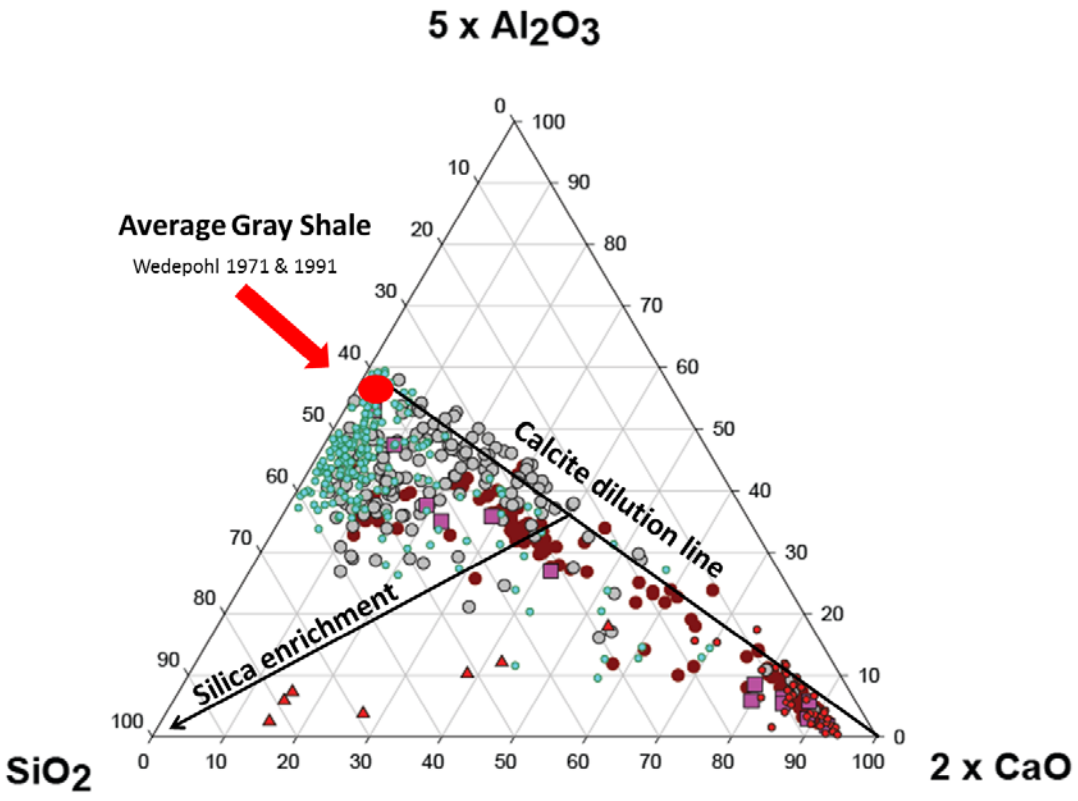

Figure 3.11 Ternary diagram for Pioneer #1 core; Calcium oxide (2 x Ca0), Alumina (5 x Al_2O_3), and Silica (SiO_2).

A cross-plot of %Si versus %Al (Figure 3.12) reveals a general trend line to the Illite/clay fraction, however multiple samples from Units A, Unit B, and the Forestburg Member plot above this line indicating the same trend toward silica enrichment as previously mentioned. The illite (Si/Al) line was created by plotting the average ratio of silica to aluminum that occurs throughout the Pioneer #1 core.

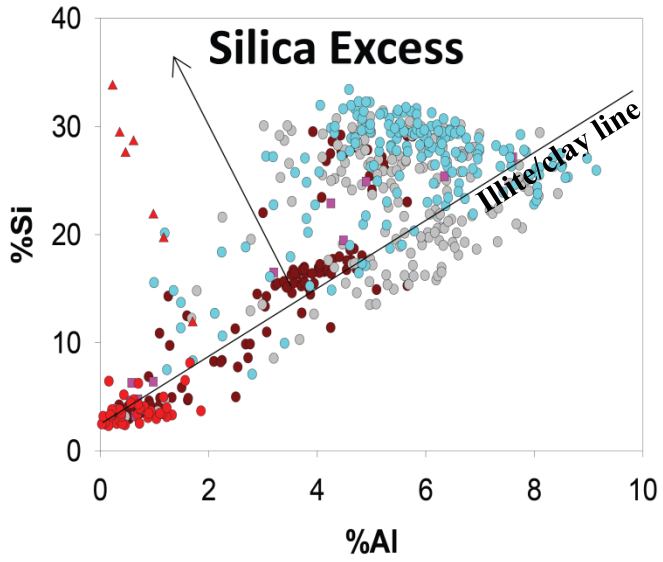

Figure 3.12 Cross-plot of silica (%) *versus* aluminum (%). Illite line = Si/Al for Pioneer #1 core.

3.2.2 Sulfur, TOC, and Iron Ternary Diagram and Cross-plots

A ternary diagram utilizing Sulfur* (S), organic carbon (TOC), and iron (Fe) end-members is used to define the amount of iron incorporated into the formation of pyrite, as well as the relative redox conditions sediments were subjected to during deposition. Values that trend toward the S/C=0.4 line are representative of sediments within a “normal marine” setting (Dean and Arthur, 1989). Figures 3.13 and 3.14 (a) illustrate linear trends with both the “pyrite” and “normal marine” lines. Multiple samples within unit A depict a slight decrease in iron toward the 100% pyrite line, while multiple unit B samples indicate an enrichment trend toward the total organic carbon fraction.

Figure 3.14 (b) is a cross-plot of %S versus %Fe. Most samples from Unit B plot above, along, or slightly below the DOP_T = 1.0 line. Most samples from Unit A plot at ~ DOP_T = .75 or below. DOP, as presented in previous works is defined as the molar ratio or pyritized iron to the whole amount of reactive iron (pyrite Fe + volatile Fe) (Berner, 1970; Raiswell et al., 1988). Such assessments were made with the use of LECO sulfur analysis. However, samples from the Pioneer #1 well were not analyzed for LECO sulfur; therefore all sulfur data presented henceforth are representative of XRF analysis. Instead of using DOP in its original form, here it is referred to as DOP_T, the molar amount of iron assumed to be in pyrite divided by the amount of total iron (Raiswell and Berner, 1986). The DOP_T levels are defined as follows: oxic (DOP_T <0.42), dysoxic (0.46<DOP_T <0.80), and anoxic/euxinic (0.55<DOP_T<0.93) (Raiswell and Berner, 1986; Raiswell et al., 1988).

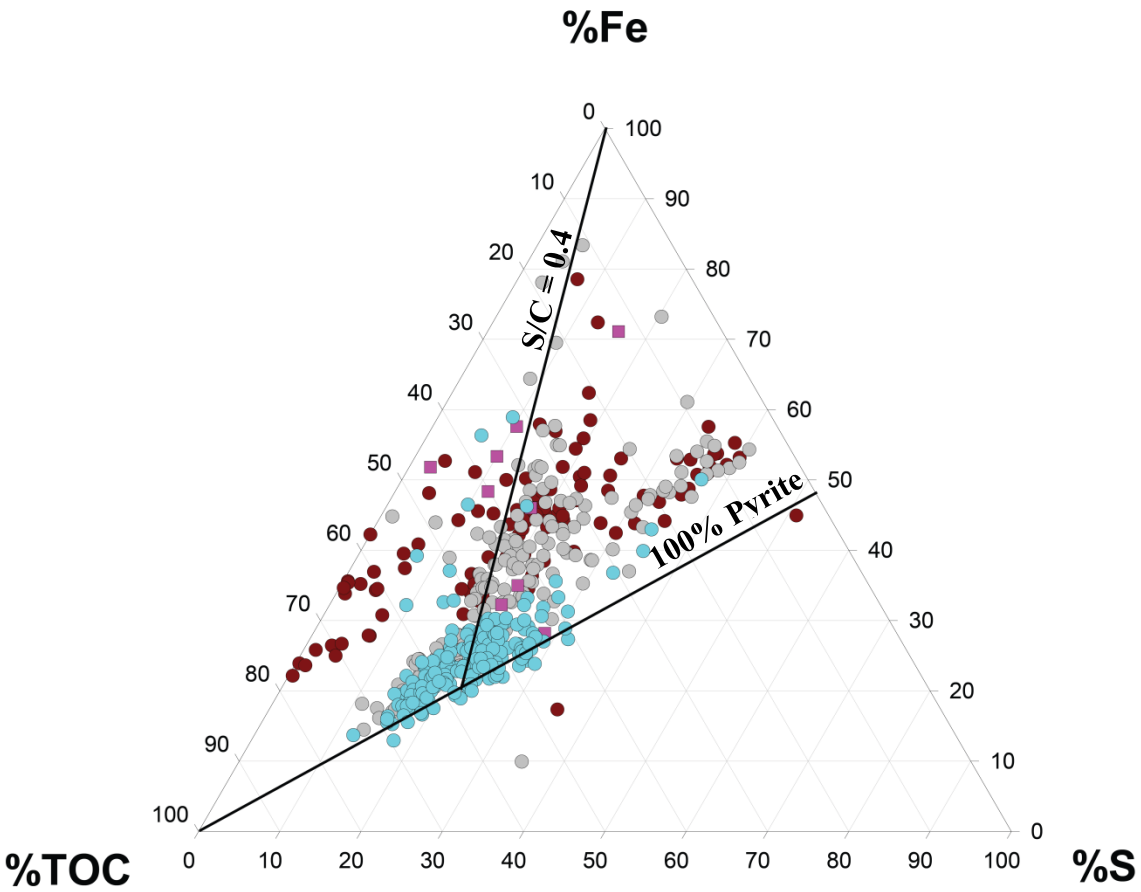

Figure 3.13 S-TOC-Fe ternary diagram for Pioneer #1 core.

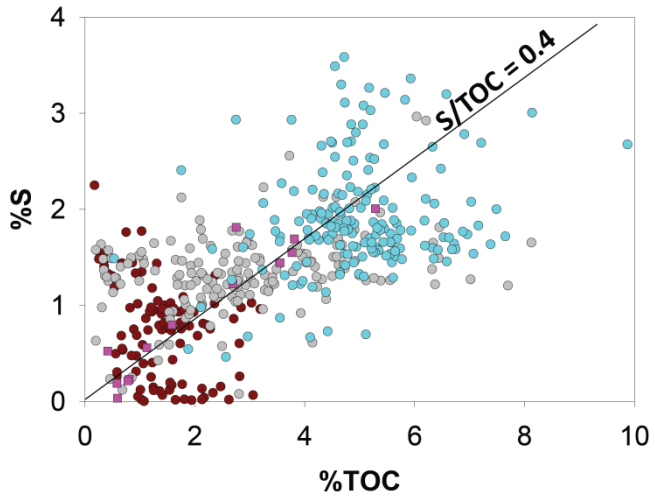

(a)

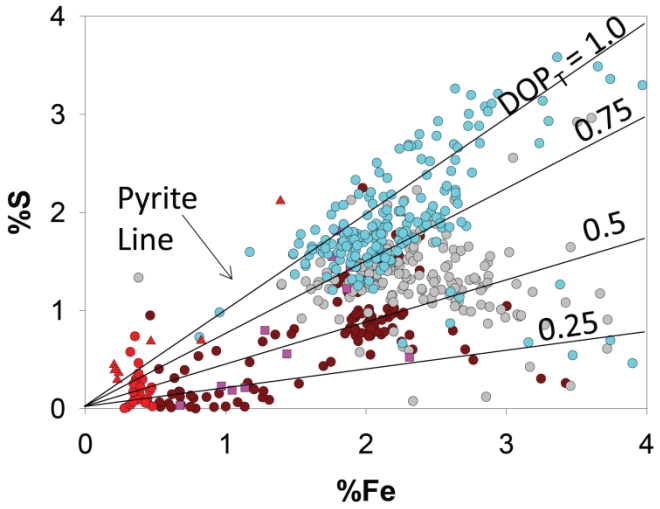

(b)

Figure 3.14 Sulfur cross-plots: a) cross-plot of sulfur (%) *versus* iron (%) with degree of pyritization slope curves (DOP_T 1.0 – 0.25) b) cross-plot of sulfur (%) *versus* TOC (%) with S/TOC slope line of 0.4 indicating normal oxic conditions above the line and anoxic to euxinic conditions below the line.

Figures 3.15 a, b, and c are also used to indicate paleo-redox conditions. Results demonstrate that samples from Unit B range in DOP_T values from ~0.6 to 1.2, while samples from Unit A range from ~0.5 to 0. Samples that depict the highest levels of both molybdenum and TOC are located within Unit B and appear to be deposited in restricted to anoxic conditions. Samples from Unit A reveal some degree of oxygen restriction as well; however samples from the Forestburg Member appear to have been deposited under more oxygenated conditions.

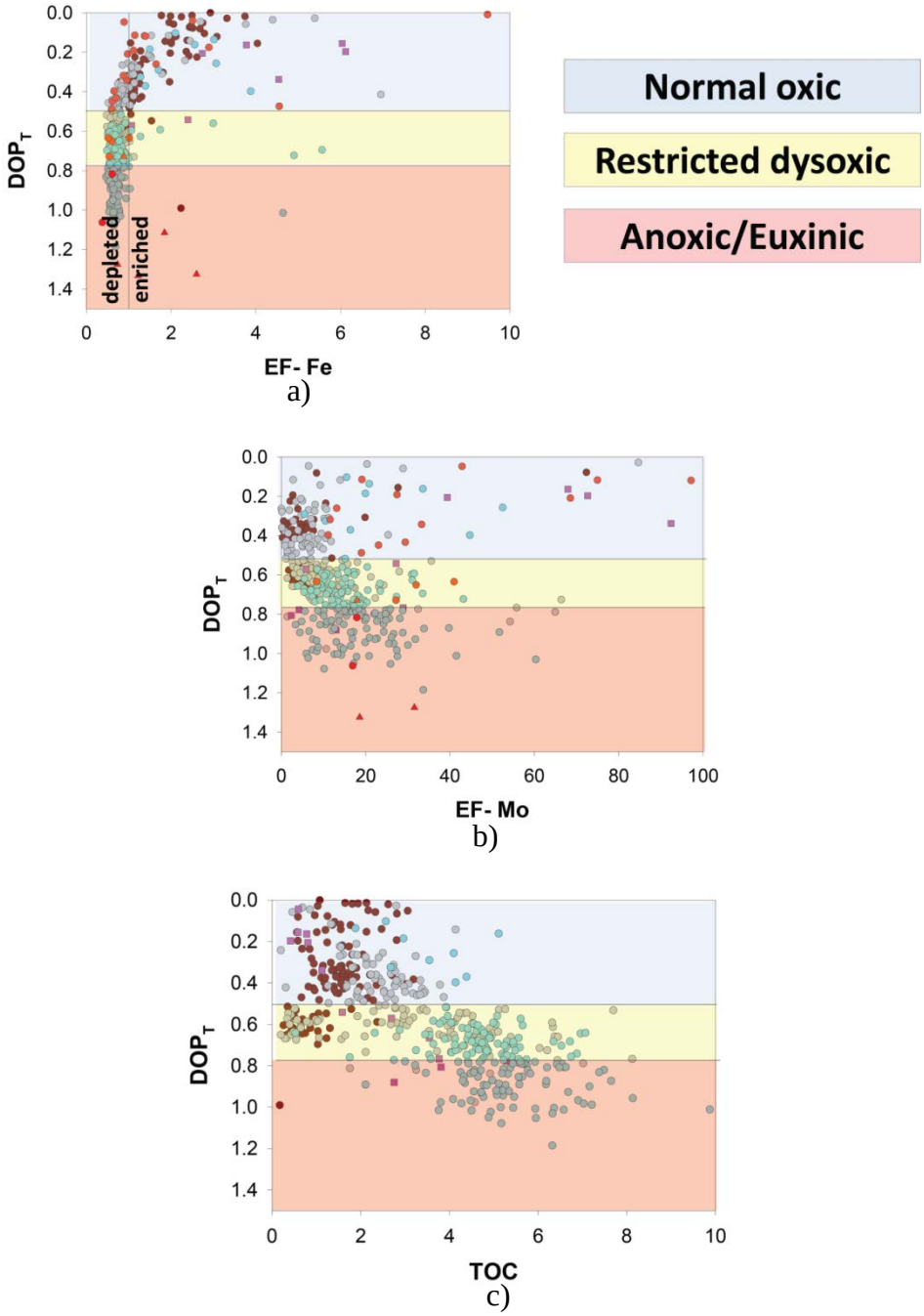

Figure 3.15 DOP_T cross-plots: a) DOP_T *versus* enrichment factor of iron, b) DOP_T *versus* enrichment factor of molybdenum, and c) DOP_T *versus* TOC for the Pioneer #1 core.

CHAPTER 4

DISCUSSION

4.1 Bulk Geochemistry

The bulk geochemistry of the Pioneer #1 well is useful in classifying the overall bulk mineralogy of the formations present. As mentioned previously, cross plots of major elements (e.g. %Si, %Fe, %Al, and %K) with aluminum are used to identify the elements that are related to the clay (illite) fraction of the sediments. Cross plots of %Ca, %Mn, Sr (ppm) and %Fe *versus* total inorganic carbon (TIC) are used to determine if these elements are related to the carbonate fraction of the sediments.

4.1.1 Major Elements

A strong linear trend is present between potassium and titanium with aluminum (Figures 4.1 (a) and (b)). These strong relationships are indicative of the presence of these elements within the clay mineral phase. The cross-plot of potassium *versus* aluminum shows a slight potassium difference between the unit A and unit B samples. This indicates unit A samples are slightly enriched in potassium *versus* unit B samples. This enrichment is also seen in the Pioneer #1 gamma ray log. Unit A samples show a slightly lower gamma ray reading than unit B samples (Figure 3.1).

The cross plot of iron *versus* aluminum (Figure 3.3) shows a linear trend suggesting that iron resides in the clay mineral phase (Table 2). Although there is a linear trend with iron, samples plotting above the trend depict a slight enrichment in iron suggesting that these samples represent the presence of iron in a separate mineral phase. The cross plot of iron *versus* total inorganic carbon (TIC) (Figure 3.8 (b)) also demonstrated a sub-linear trend

indicating that iron may also have a relationship with a carbonate phase, possibly in the formation of siderite and/or ferroan dolomite.

In order to further delineate the iron to carbonate fraction, iron was normalized to the clay fraction of the sediments by plotting a ratio of iron to aluminum (Fe/Al) (Figures 3.6 a, b, and c). Therefore, any enrichment in iron after such normalization is made indicates an enrichment that is assumed to be unrelated to the clay fraction of the sediments. The moderate trend represented in figure 4.3 a further suggests that iron is indeed related to the carbonate phase, while the relationship represented in figure 4.3 c depicts the presence of an iron sulfide phase (e.g. pyrite) in predominantly unit B and possibly unit A. Visual inspection of the Pioneer #1 core reveals the presence of pyrite within the Barnett Formation.

Cross plots of silica *versus* aluminum (Figure 3.12) depict a linear trend; however, multiple data points lie above the trend line, indicating the presence of an excess amount of silica. In order to define such enriched samples, an illite (Si/Al) line was created by plotting the average ratio of silica to aluminum that occurs throughout the Pioneer #1 core. Therefore, data points that lie above the illite Si/Al line indicate enrichment in silica relative to the clay fraction. This enrichment is indicative of silica being present in other mineral phases such as biogenic silica (radiolarians) and/or detrital quartz.

4.1.2 Carbonate Mineralogy

Total inorganic carbon, as previously mentioned in chapter 3, is often used as a geochemical proxy for carbonate phases such as calcite (Table 2). There is a strong linear trend with calcium and total inorganic carbon suggesting such a proxy (Figure 3.8 a). However, multiple samples plot both above and below the carbonate trend line suggesting calcium is also present in other mineral phases and TIC is also associated with separate mineral phases, other than calcite.

The cross-plot of calcium *versus* phosphate (Figure 3.4) does not indicate a linear trend suggesting its presence is not related to the carbonate phase. However, upon visual inspection of the Pioneer #1 core, the presence of multiple phosphate nodules at the transition zone between the lower Barnett and the Viola Limestone are common. Similarly, previously published works found phosphatic layers and nodules present within the core (Loucks and Ruppel, 2008; Loucks, 2009).

The magnesium *versus* calcium cross-plot illustrates a relationship between the two elements in two separate phases (Figure 3.8 (c)). Samples from both unit A and unit B represent a dilution trend with magnesium indicating a slight presence in the strata. However, samples from both the overlying Forestburg and underlying Viola/Simpson Group indicate the highest degree of magnesium enrichment. This trend suggests the presence of dolomite within these particular units of the core.

4.1.3 Bulk Mineralogy and Well log correlation

Previously mentioned bulk mineralogical changes seen throughout the Pioneer #1 core were also plotted in down-core plots to analyze any possible correlation to changes seen in the total gamma ray well log. It is well known that the gamma ray tool measures the presence of radioactive elements such as potassium, uranium and thorium. A concentration of any/all of these elements will create an increase in the gamma ray response (positive excursion), while a lesser amount of such elements will created a decrease in the gamma ray log (negative excursion). Previously discussed plots of both potassium and thorium *versus* aluminum indicate a strong relationship suggesting such elements resides in the clay fraction. Therefore, it is to be expected that clay-rich rocks will create an increase in the gamma ray response, while clay poor sediments will cause a decrease.

Observations from the gamma ray log indicate the presence of two coarsening upward packages of sediment located in both unit A and unit B; as seen by the upward progressive

decrease in the gamma ray counts. Such coarsening upward packages indicate a general decrease in the amount of clay present in the strata and suggest a larger presence of other elements such as calcium and silica. The base of unit B (highlighted in grey) begins with a high gamma ray response which corresponds to an overall increase in the %Al plot and a decrease in Si/Al. Moving up-core, the gamma ray continuously decreases in gamma ray counts. The geochemistry displays the same results with a decrease in %Al and an increase in Si/Al. This suggests that unit B is enriched in silica relative to the clay fraction, as previously discussed. Calcium also shows abrupt shifts of enrichment within unit B that correspond to abrupts shifts in %TIC. These shifts are also denoted on the gamma ray log by slightly decreasing spikes. These enrichments in %Ca and %TIC may be interpreted as small scale density flows from the basin shelf.

Unit C is denoted in the gamma ray log by an abrupt negative excursion. This decrease corresponds to sudden increases in %Ca, %TIC, and Si/Al. An increase in either %Ca or Si/Al separately may suggest carbonate deposition, high biogenic silica production and preservation, or large amounts of detrital sedimentation to the basin. However, there is a sudden increase in both calcium and silica concurrently. A probable explanation for such occurrence is the preservation of a larger-scale density flow from the adjacent shelf. Such phenomenon has the capability of depositing multiple types of sediments together to distal regions of the basin.

Rocks comprised in unit A represent the second coarsening upward package preserved in the Pioneer #1 core. This unit begins with a high gamma ray reading corresponding to an increase in %Al and decrease in Si/Al. This unit progressively coarsens upwards into a calcium rich layer (highlighted in blue). These sediments display a rapid increase in %Ca and %TIC, suggesting a carbonate rich provenance. Sediments capping unit A are enriched in silica and depleted in calcium and TIC. This suggests a possible switch in sediment sourcing to the basin from a calcium rich provenance to a silica rich provenance.

4.2 Paleoceanography

4.2.1 Physical Paleoceanography

It is a general conclusion that the Barnett was deposited under anoxic to euxinic conditions with relatively high amounts of organic matter accumulations (e.g.Loucks and Ruppel, 2007; Rowe et al., 2008; Algeo and Rowe, 2011). Due to the degree of restriction within the basin, deepwater renewal times were very long. When deepwater renewal is long, trace metal concentrations become very limited in resupply. Under such conditions, concentrations of trace metals tend to become proportional to the levels of organic carbon. Therefore, the ratio of trace metals to total organic carbon may be used as a proxy to determine the degree of basin restriction (Algeo and Lyons, 2006).

A geochemical study of the Barnett Formation (Rowe et al., 2008), suggested that the Mo-TOC ratio for the Barnett Formation indicated a degree of basin restriction greater than that of the Black Sea (Figure 4.8 a). Samples from the Pioneer #1 well (Figure 4.8 b) demonstrate the same degree of restriction. These results also determine sediments from unit B preserve the highest amount of total organic carbon suggesting the highest degree of restriction, highest amount of preservation, or highest levels of productivity may have occurred during the time of unit B deposition.

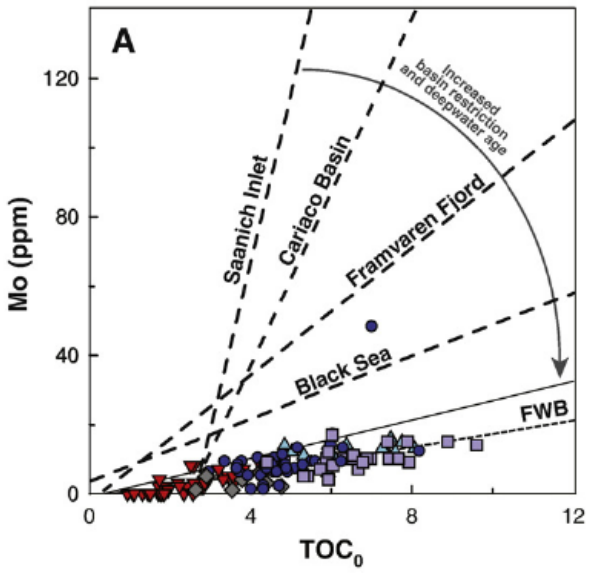

(a)

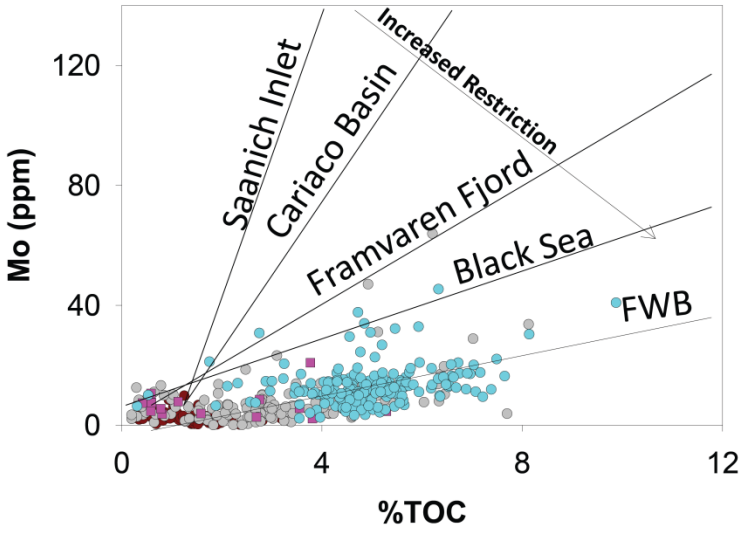

(b)

Figure 4.1 Figure depicting the Mo-TOC ratio for the Barnett Formation (A) from the Texas United 1 Blakely core (Rowe et al., 2008) and (B) from the Pioneer #1 well.

The geometry of the FWB during Barnett deposition is not very well known or understood due to the hypothetical nature of paleogeographic reconstructions. However, it is well documented that the Fort Worth Basin was restricted to the open Rheic Ocean due to the presence of multiple tectonic elements (e.g. Caballos-Arkansas Island Chain and Gondwana). Due to the presence of such tectonic elements, it is possible that a shallow sill could have been present around the FWB basin during the Mississippian time period creating the high degree of basin restriction that is recorded in the Pioneer #1 stratum.

4.2.2 Chemical Paleoceanography

Relationships between sulfur, iron, and organic carbon may be used to evaluate the paleoredox conditions in the FWB during the time of Barnett deposition. A cross-plot of sulfur *versus* iron was used to determine the association of iron with sulfur (Figure 3.14 (b)). A linear trend along the pyrite line (DOP_T = 1.0) with sediments from unit B indicates the presence of iron in a sulfidic phase (e.g. pyrite). Samples falling below that line determine the degree of iron in pyrite. A cross-plot of sulfur *versus* total organic carbon (TOC) (Figure 3.14 (a)) was used to define paleoredox conditions during Barnett deposition. According to Berner and Raiswell (1983), samples that plot along a line with a positive slope of 0.4 and a y-intercept of zero indicate deposition under normal marine conditions, where samples that do not define a positive correlation between S/TOC = 0.4 line indicate possible deposition under anoxic or euxinic conditions. Most samples from unit A plot above the S/TOC = 0.4 line indicating normal marine conditions, where multiple samples from unit B plot along or below the line indicating anoxic to euxinic conditions.

A second method presented by Raiswell and Berner (1986) and Raiswell et al. (1988) utilizes the degree of pyritization (DOP_T) to determine bottom water redox conditions. DOP_T levels in the Pioneer #1 well range from oxic to anoxic/euxinic redox conditions. Samples from unit B represent the highest degree of anoxia to euxinia, while samples from unit A were

deposited under a range of redox conditions from normal oxic to dysoxic. The high levels of DOP_T seen within unit B are likely the result of persistent anoxic conditions with episodes of euxinia.

Cross-plots of DOP_T *versus* iron enrichment, molybdenum enrichment, and total organic carbon were also assessed to determine their relationship with redox conditions (Figure(s) 3.15 a, b, and c). The cross-plot of DOP_T *versus* EF-Fe determines that the strata within unit B underwent the highest degree of redox conditions as well as revealing these rocks have an overall depletion in iron, while sediments deposited in more oxic conditions, unit A, are relatively enriched in iron. The cross-plot of DOP_T *versus* EF-Mo displays a general relationship between iron sulfurization and the enrichment of molybdenum. Samples from unit B depict, again, the highest DOP_T as well as the highest levels of molybdenum sequestration. These results reveal that the strata from unit B underwent the highest degree of basin restriction. Lastly, a cross-plot between DOP_T and TOC was used to assess the relationship between basin restriction and TOC accumulation and preservation. The strong relationship seen between these two variables (Figure 3.15 (c)) suggests that strata undergoing the highest degree of restriction also preserve the highest amounts of TOC. Such rocks within the Pioneer #1 well are located in unit B.

CHAPTER 5

CONCLUSIONS

5.1 Conclusions

The use of geochemistry and chemostratigraphy has further assessed the paleogeography and paleoceanography of the Fort Worth Basin during the time of Barnett Formation deposition. Paleoredox conditions preserved in the Pioneer #1 core have provided new insight into the paleoceanography of the northern most extents of the FWB. Geochemistry has also provided new methods for reconstructing the chemostratigraphic boundaries of the Barnett Formation.

1. The physical and geochemical assessment of the Pioneer #1 core has revealed that Barnett Formation strata of the northern Fort Worth Basin were deposited in a restricted marine setting. The relatively high degree of basinal restriction created longer deepwater renewal times than that of the Black Sea and therefore led to lower trace metal enrichments and high levels of organic carbon preservation.

2. The bulk geochemistry of the Pioneer #1 core revealed both silica enrichments as well as a calcium enrichment in Barnett strata. These enrichments suggest two separate sediment provenances to the northern Fort Worth Basin.

3. Chemostratigraphy, along with well log readings, of the Pioneer #1 core correlated to two upward coarsening sequences within two units of the lower Barnett Formation.

4. The DOP_T that occurred within the northern Fort Worth Basin revealed that rocks within the Pioneer #1 core were deposited in oxygen stratified waters. Unit B displays the

5. highest degree of euxinia while sediments from unit A were deposited under more oxygenated conditions.

6. TOC analysis, along with redox indicators, determined the most organic accumulation and preservation occurred within unit B sediments. Therefore, these strata would be expected to have the highest production potential within the northern FWB.

REFERENCES

Algeo, T.J. and Lyons, T.W., 2006. Mo-total organic carbon covariation in modern anoxic marine environments: implications for analysis of paleoredox and paleohydrographic conditions. Paleoceanogaphy, v. 21, PA1016.

Algeo, T.J., Lyons, T.W., Blakey, R.C., and Over, D.J. 2007. Hydrographic conditions of the Devono-Carboniferous North American Seaway inferred from sedimentary Mo-TOC relationships. Palaeogeograhy, Palaeoclimatology, Palaeoecology. 256: 204-230.

Algeo, T.J., Maynard, J.B., 2008. Trace-metal covariation as a guide to water-mass conditions in ancient anoxic marine environments. Geosphere. Oct 2008, v. 4, no. 5; 872-887.

Algeo, T.J. and Tribovillard, N. 2009. Environmental analysis of paleoceanographic systems based on molybdenum-uranium covariation. Chemical Geology. 268: 211-225.

Algeo, T.J. and Rowe, H. 2011. Paleoceanographic applications of trace-metal concentration data. Chemical Geology. Vol. 324-325. pp. 6-18.

Aplin, A.C., Fleet, A.J., and Macquaker, J.H.S. 1999. Muds and mudstones: physical and fluid-flow properties. Geological Society, London, Special Publications, v. 158: 1-8.

Arbenz, J.K., 1989, The Ouachita system, in A.W. Bally and A.R. Palmer, eds., The geology of North America – An overview: Geological Society of America, The Geology of North America, v. A, P. 371-396.

Arthur, M.A., Sageman, B.B., 1994. Marine black shales: depositional mechanisms and environments of ancient deposits. Annual Reviews in Earth and Planetary Sciene. 22: 499-551.

Berner, R.A. 1970. Sedimentary pyrite formation. American Journal of Science. 268: 1-23

Berner, R.A. and Raiswell, R., 1983. Burial of organic carbon and pyrite sulfur in sediments over Phanerozoic time: a new theory. Geochimica et Cosmochimica Acta. 47: 855-862.

Blakey, R., 2005. Paleogeography and geologic evolution of North America; images that track the ancient landscapes of North America: http://jan.ucc.nau.edu/~rcb7/nam.html (accessed June 17, 2011).

Blatt, H., 1970. Determination of mean sediment thickness in the crust: a sedimentologic method. Geologic Society of Americal. Vol. 81: 255-262.

Blatt,H., 1985. Provenance Studies and Mudrocks. Journal of Sedimentary Petrology. Vol.55, No.1: 69-75.

Boardman, Darwin R. II, Beuthin, Jack D., and William, Eliott S. Jr. 2012. Chronostratigaphic and Sedimentological interpretation of the Barnett Shale (Mississippian) of the Llano Uplift and Fort Worth Basin, Texas. AAPG Search and Discovery Article # 50635.

Calvert, S.E. and Pedersen, T.F. 1993. Geochemistry of recent oxic and anoxic marine sediments: implications for the geological record. Marine Geology. 113: 67-88.
Crusius, J., Calvert, S., Pedersen, T., Sage, D., 1996. Rhenium and molybdenum enrichments in sediments as indicators of oxic, suboxic and sulfidic conditions of deposition. Earth and Planetary Science Letters. 145: 65-78.

Cortez, Milton III, 2012. Chemostratigraphy, paleoceanography, and sequence stratigraphy of the Pennsylvanian-Permian section in the Midland Basin of West Texas, with focus on the Wolfcamp formation. M.Sc. Thesis. University of Texas at Arlington: USA.

Dean, W.E and Arthur, M.A. 1989. Iron-sulfur-carbon relationships in organic-carbon-rich sequences I: Cretaceous western interior seaway. American Journal of Science. 289:708-743.
Gutschick, R., and C. Sandberg, 1983, Mississippian continental margins on the conterminous United States, in D.J. Stanley and G.T. Morre, The shelf break: Critical interface on continental margins: SEPM Special Publication 33, p. 79-96.

Engleman, E.E., Jackson, L.L., Norton, D.R. and Fischer, A.G. 1985. Determination of carbonate carbon in geological materials by coulometric titration. Chemical Geology. 53: 125-128.

Henry, J.D. 1982. Stratigraphy of the Barnett Shale (Mississippian) and associated reefs in the northern Fort Worth Basin, in Martin, C.A., ed., Petroleum Geology of the Fort Worth Basin and Bend Arch Area: Dallas Geological Society, p. 157-178.

Hill, R.J., Jarvie, D.M., Sumberge, J., Henry, M., and Pollastro, R.M. 2007. Oil and gas geochemistry and petroleum systems of the Fort Worth Basin. AAPG Bulletin. vol. 91, no. 4. pp. 445-473.

Hughes, E.N., Rowe, H.D., Ruppel, S., and Loucks, R. 2009. Geochemistry of the Barnett Formation from three Texas Hill Country cores (in Geological Society of America, South-Central Section, 43rd annual meeting, Anonymous) Abstracts with Programs – Geological Society of America (March 2009), 41(2):7.

Hoelke, James D., 2011. Chemostratigraphy and paleoceanography of the Mississippian Barnett Formation, southern Fort Worth Basin, Texas, USA. M.Sc. Thesis. University of Texas at Arlington: USA.

Jarvie, D.M., Hill, R.J., Ruble, T.E., and Pollastro, R.M. 2007. Unconventional shale-gas systems: The Mississippian Barnett Shale of north-central Texas as one model for thermogenic shale-gas assessment. AAPG Bulletin. vol. 91, no. 4. pp. 475-499.

Jones, B. and Manning, D.A.C., 1994. Comparison of geochemical indices used for the interpretation of paleoredox conditions in ancient mudstones. Chemical Geology. 111: 111-129.

Kier, R.S., Brown Jr., L.F., and McBride, E.F. 1979. The Mississippian and Pennsylvanian (Carboniferous) Systems in the United States – Texas. U.S. Geological Survey Professional Paper 1110-S.

Leithold, E.L., 1994. Stratigraphical architecture at the muddy margin of the Cretaceous Western Interior Seaway, southern Utah: Sedimentology. vol. 41. pp. 521-542.

MacQuaker, J.H.S. and Gawthorpe, R.L., 1993. Mudstone lithofacies in the Kimmeridge Clay Formation, Wessex Basin, Southern England: Implications for the origin and controls of the distribution of mudstones. Journal of Sedimentary Petrology. vol. 63. no. 6. pp. 1129-1143.

Loucks, R.G. and Ruppel, S.C. 2007. Mississippian Barnett Shale: Lithofacies and depositional setting of a deep-water shale-gas succession in the Fort Worth Basin, Texas. AAPG Bulletin, vol. 91, no. 4; 579-601.

Loucks, R.G. and Ruppel, S.C. 2008. The Barnett Shale of the southern Fort Worth Basin; comparison of depositional setting, lithofacies, and mineralogy with equivalent deposits in the northern basin. Abstracts: Annual Meeting – American Association of Petroleum Geologists.

Maiz, N. 2007. Geochemical characterization of gases from the Barnett Shale, Fort Worth Basin, Texas. Master's Thesis: University of Oklahoma. 123pp.

Montgomery, S.L., Jarvie, D.M., Bowker, K.A., and Pollastro, R.M. 2005. Mississippian Barnett Shale, Fort Worth Basin, northcentra Texas: Gas-shale play with multi-trillion cubic foot potential. AAPG Bulletin. vol. 89. p. 155-175.

Morford, J.L. and Emerson, S. 1999. The geochemistry of redox sensitive trace metals in sediments. Geochimica et Cosmochimica Acta. Vol. 63, No. 11/12, pp. 1735-1750.

Meyers, P.A. and Eadie, B.J. 1993. Sources, degradation and recycling of organic matter associated with sinking particles in Lake Michigan. Organic Geochemistry. Vol. 20, No.1, pp. 47-56.

Meyers, P.A. 1994. Preservation of elemental and isotopic source identification of sedimentary organic matter. Chemical Geology. 114: 289-302.

Meyers, P.A. 1997. Organic geochemical proxies of paleoceanographic, paleolimnologic, and paleoclimatic processes. Organic Geochemistry. Vol. 27, No. 5/6, pp 231-250.

Meyers, P.A., Bernasconi, S.M., and Forster, A. 2006. Origins and accumulation of organic matter in expanded Albian to Santonian black shale sequences on the Demerara Rise, South American margin. Organic Geochemistry. 37: 1816-1830.

Piper, D.Z. 1994. Seawater as the source of minor elements in black shales, phosporites and other sedimentary rocks. Chemical Geology. 114: 95-114.

Pollastro, R.M., Jarvie, D.M., Hill, R.J., Adams, C.W., 2007. Geologic framework of the Mississippian Barnett Shale, Barnett-Paleozoic total petroleum system, Bend arch-Fort Worth Basin, Texas. AAPG Bulletin, vol. 91, no. 4; 405-436.

Potter, P.E., Maynard, J.B. and Pryor, W.A. 1980. Sedimentology of Shale: New York, Springer Verlag. 306 p.

Potts, Philip J. and Webb, Peter C. 1992. X-ray fluorescence Spectromety. Journal of Geochemical Exploration. 44: 251-296.

Raiswell, R. and Berner, R.A. 1986. Pyrite and organic matter in Phanerozoic normal marine shales. Geochimica et Cosmochimica Acta. 50: 1967-1976.

Raiswell, R., Buckley, F., Berner, R.A., and Anderson, T.F. 1988. Degree of pyritization of iron as a paleoenvironmental indicator of bottom-wateroxygenation. Journal of Sedimentary Petrology. 58: 812-819.

Rimmer, S.M., Thompson, J.A., Goodnight, S.A., and Robl, T.L. 2004. Multiple controls on the preservation of organic matter in Devonian-Mississippian marine black shales: geochemical and petrographic evidence. Palaeogeography, Palaeclimatology, Palaeoecology. 215: 125-154.

Rodriguez, R.D. and Philp, R.P. 2010. Geochemical characterization of gases from the Mississippian Barnett Shale, Fort Worth Basin, Texas. AAPG Bulletin. vol 94. no. 11. pp. 1641-1656.

Ross, C.A. and Ross, J.R.P. 1987. Late Paleozoic sea levels and depositional sequences, in C.A. Ross and D. Haman, eds., Timing and deposition of eustatic sequences: Constraints on seismic stratigraphy: Cushman Foundation for Foraminiferal Research Special Publication. 24: 137-149.

Rosseau, R.M. 2001. Detection limit and estimate of uncertainty of analytical XRF results: The Rigaku Journal. 18: 33-47.

Rowe, H.C., Loucks, R.G., Ruppel, S.C., Rimmer, S.M., 2008. Mississippian Barnett Formation, Fort Worth Basin, Texas: Bulk geochemical inferences and Mo-TOC constraints on the severity of hydrographic restriction. Chemical Geology. 257: 16-25.

Rowe, H.D.; Ruppel, S.; Rimmer, S.; Loucks, R.G., 2009. Core-based chemostratigraphy of the Barnett Shale, Permian Basin, Texas. Gulf Coast Association of Geological Societies Transactions. 59: 675-686.

Rowe, H. D., Hughes, N., and Robinson, K., 2012. The quantification and application of handheld energy-dispersive x-ray fluorescence (ED-XRF) in mudrock chemostratigraphy and geochemistry. Chemical Geology 324-325, 122-131.

Schieber, J., and Zimmerle, W. 1998. Introduction and overview: The history and promise of shale research, in J. Schieber, W. Zimmerle, and P. Sethi, eds., Shales and Mudstones I: Stuttgart, Germany, E. Schweizerhbart'sche Verlagsbuchhandlung, p. 1-10.

Slatt, R.M., 2002. Significance of Shales and Mudrocks in Oil and Gas Exploration and Reservoir Development. Gulf coast Association of Geological Societies Transactions. Vol. 52: 1119-1130.

Tai, David W.N. 1979. Subsurface Study of Atoka (Lower Pennsylvanian) clastic rocks in parts of Jack, Palo Pinto, Parker, and Wise Counties, North-Central Texas. AAPG, vol. 63, no 1. pp. 50-66.

Thompson, D.M. 1988. Fort Worth basin. In: Sloss, L.L. (Ed.), The Geology of North America, D-2. Geological Society of America, 99. 346-352.

Tribovillard, N., Algeo, T.J., Lyons, T., and Riboulleau, A. 2006. Trace metals as paleoredox and paleoproductivity indicators: an update. Chemical geology. 232: 12-32.

Twichell, S.C., Meyers, P.A., and Diester-Haass, L. 2002. Significance of high C/N ratios in organic-carbon-rich Neogene sedients under the Benguela Current upwelling system. Organic Geochemistry. 33: 715-722.

Verardo, D.J., Froelich, P.N., and McIntyre, A. 1990. Determination of organic carbon and nitrogen in marine sediments using the Carlo Erba NA-1500. Deep-Sea Research. 37: 157-165.

Vine, J.D. and Tourtelot, E.B., 1970. Preliminary geochemical and petrographic analysis of lower Eocene fluvial sandstones in the Rocky Mountain Region. Wyoming Geological Association. 22nd Annual Field Congerence Guidebook. pp. 251-263.

Walper, J.L., 1977. Paleozoic Tectoics of the Southern Margin of North America. Gulf coast Association of Geological Societies Transactions. vol. 27: 230-241.

Walper, J.L., 1982. Plate tectonic evolution of the Fort Worth Basin. In: Martin, C.A. (Ed.), Petroleum Geology of the Fort Worth Basin and Bend Arch Area. Dallas Geological Society, pp. 237-251.

Wedepohl, K.H., 1971. Environmental influences on the chemical composition of shales and clays. In: Ahrens, L.H., Press, F., Runcorn, S.K., Urey, H.C. (Eds.), Physics and Chemistry of the Earth vol. 8, Pergamon, Oxford (1971), pp. 305-333.

Wedepohl, K.H., 1991. The composition of the upper earth's crust and the natural cycles of selected metals. Metals in natural raw materials. Natural Resources. In: Merian, E. (Ed.), Metals and Their Compounds in the Environment. VCH, Weinheim, pp. 3-17.

Wilkin, R.T., Barnes, H.L., and Brantley, S.L. 1996. The size distribution of framboidal pyrite in modern sediments: an indicator of redox conditions. Geochemica et Cosmochimica Acta. 60: 3897-3912.

Wilkin, R.T., Arthur, M.A., and Dean, W.E. 1997. History of watercolum anoxia in the Black Sea indicated by pyrite framboids size distributions. Earth and Planetary Science Letters. vol. 148, p. 517-525.

BIOGRAPHICAL INFORMATION

Krystin Chantel Robinson was born on August 4, 1985 in Hurst, Texas. Krystin grew up in Hurst, Texas and graduated from Lawrence D. Bell High School in 2003. She attended the University of Texas at Arlington where she earned a Bachelor of Science degree in Geology in May 2011. After graduation, she went straight into working on her Master's Degree. She again attended the University of Texas at Arlington where she entered the Master of Science program under the supervision of Dr. Harry Rowe. She is scheduled to complete her Master's degree in Geology in 2012 where after she will begin her career in industry.